

1 **Geochemistry of the Phlegraean Fields (Italy) proximal sources for major**
2 **Mediterranean tephras: implications for the dispersal of Plinian & co-**
3 **ignimbric components of explosive eruptions**

4
5 Emma L. Tomlinson^{1*}, Ilenia Arienzo², Lucia Civetta^{2,3}, Sabine Wulf⁴, Victoria C.
6 Smith⁵, Mark Hardiman⁶, Christine S. Lane⁵, Antonio Carandente², Giovanni
7 Orsi², Mauro Rosi⁷, Wolfgang Müller¹, Matthew F. Thirlwall¹ and Martin A.
8 Menzies¹

9
10 ¹Department of Earth Sciences, Royal Holloway University of London, Egham,
11 U.K.

12 ²Istituto Nazionale di Geofisica e Vulcanologia, sezione di Napoli-Osservatorio
13 Vesuviano, Napoli, Italy.

14 ³Dipartimento di Scienze Fisiche, Università di Napoli Federico II, Napoli, Italy.

15 ⁴GFZ German Research Centre for Geosciences, Section 5.2 – Climate
16 Dynamics and Landscape Evolution, Potsdam, Germany

17 ⁵Research Laboratory for Archaeology and the History of Art, University of
18 Oxford, Oxford, United Kingdom

19 ⁶Centre of Quaternary Research, Department of Geography, Royal Holloway
20 University of London, Egham, Surrey, United Kingdom.

21 ⁷Dipartimento di Scienze della Terra, Università di Pisa, Pisa, Italy.

22
23 **ABSTRACT**

24
25 Volcanic activity at Phlegraean Fields, Italy, produced several major marker
26 tephras over a 50 ka period. The caldera forming eruptions of the Campanian
27 Ignimbrite (CI) and Neapolitan Yellow Tuff (NYT) are of particular importance for
28 tephrostratigraphy in Europe. Other key eruptions from this source include the
29 Pomici Principali (PP) and the Tufi Biancastri eruptions. We combine analyses of
30 fresh glasses from proximal locations (i.e., juvenile clasts in proximal flow and fall
31 deposits) with data for key tephra layers from Lago Grande di Monticchio, 120 km
32 to the east. The micron-beam major (EMPA) and trace (LA-ICP-MS) element
33 glass dataset allows us to: (a) Distinguish between tephra units produced from
34 the Phlegraean Fields before and during the CI eruption (CI-series), and before
35 and during the NYT and PP eruptions (NYT-series/PP); (b) Discriminate between
36 the CI and the geochemically similar Pre-CI pyroclastic deposits; (c) Separate the
37 NYT from Pre-NYT tephra units, although both major and trace elements do
38 show significant overlap. The complex compositional overlap between Pre-NYT
39 tephras may present a problem for tephra correlations in the 14-39 ka time
40 window and may have resulted in incorrect proximal-distal and distal-distal
41 correlations. The diagnostic chemical criteria detailed herein permits more
42 accurate matching of distal tephras with their proximal equivalents and hence will
43 improve chronostratigraphy of distal settings and give insight into tephra
44 dispersal. We show that the dispersal of PP tephra was more limited than
45 previously thought. The surge/fall (Lower Member) and subsequent pyroclastic
46 density current (Upper Member) phases of the NYT eruption can be recognised

47 in distal settings. Both the NYT Lower and Upper Members are found in distal
48 localities to the east of the Phlegraean Fields, however the Lower Member is
49 found in the absence of the Upper Member in locations to the far north of
50 Phlegraean Fields. Chemical compositions of the Plinian and ignimbrite phases
51 of the CI eruption overlap extensively, but can be distinguished on a plot of Zr-Th.
52

53 **Key Words: Tephrostratigraphy, LA-ICP-MS, Campi Flegrei, Campanian**
54 **Ignimbrite, Neapolitan Yellow Tuff, Lago Grande di Monticchio**

55

56 1. INTRODUCTION

57

58 Tephra layers deposited during large explosive volcanic eruptions form important
59 isochronous marker beds in the stratigraphic record, allowing correlation between
60 archaeological, terrestrial, marine and ice records (tephrostratigraphy). In
61 addition, if the tephra can be correlated to a source and age of the eruption is
62 well established, distal ash layers can be used as age markers within the
63 stratigraphic record (tephrochronology). Furthermore, a reliable correlation
64 between proximal and distal facies of an eruption deposit allows the eruption
65 volume and tephra dispersal pattern to be reconstructed. Knowledge of these two
66 parameters is important in volcanic hazards assessments and zoning of the
67 territory in relation to the expected hazards. This is critical for active, restless and
68 densely populated volcanoes such as the Phlegraean Fields resurgent caldera
69 (Orsi et al., 1996, 1999a, b, 2004, 2009; Costa et al., 2009; Selva et al., 2012).
70

71 Tephra produced during the two most recent caldera forming eruptions at
72 Phlegraean Fields (Fisher et al., 1993; Orsi et al., 1996), the Campanian
73 Ignimbrite (CI, 39.28 ± 0.11 $^{40}\text{Ar}/^{39}\text{Ar}$ ka; De Vivo et al., 2001) and the Neapolitan
74 Yellow Tuff (NYT, 14.9 ± 0.4 $^{40}\text{Ar}/^{39}\text{Ar}$ ka; Deino et al., 2004), provide important
75 stratigraphic markers in European Quaternary deposits (e.g. Schmidt et al., 2002;
76 Fedele et al., 2003; Pyle et al., 2006; Giaccio et al., 2008). The CI was the most
77 explosive eruption of the Campanian Volcanic Zone (CVZ) and the largest known
78 volcanic event in the Mediterranean region in the last 200 ka (Barberi et al.,
79 1978). The CI has been correlated with distal occurrences of the Y-5 tephra in
80 the eastern Mediterranean, central and eastern Europe and Russia (e.g. Keller et
81 al., 1978; Thunell et al., 1979; Paterne et al., 1988; Vezzoli, 1991; Pyle et al.,
82 2006). The CI is linked with layer TM-18 (36.77 varve ka BP) in the Lago Grande
83 di Monticchio sediment core (Wulf et al., 2004). Some 25 ka later, activity in the
84 Phlegraean Fields caldera produced the NYT. The NYT has been correlated with
85 the 13.84-14.88 cal ka BP¹ C-2 tephra layer in the Tyrrhenian and Adriatic Seas
86 (Paterne et al., 1988; Calanchi et al., 1998; Siani et al., 2004; Bourne et al.,

¹ All radiocarbon ages presented here (cal ka BP) have been calibrated using the IntCal09 or Marine09 internationally accepted calibration curves (Reimer et al., 2009) at 2σ . Year 0 is 1950 AD. Please see references for uncalibrated radiocarbon determinations.

87 2010) and with TM-8 (14.12 varve ka BP) in the Lago Grande di Monticchio core
88 (Wulf et al., 2004; 2008). The smaller Pomici Principali (PP, also known as
89 Agnano Pomici Principali) eruption dated at 11.92-12.26 cal ka BP (Smith et al.,
90 2011) has been correlated with TM-7b (12.18 varve ka BP) in the Lago Grande di
91 Monticchio core (Wulf et al., 2004; 2008) and has also been described in the
92 Adriatic Sea (Paterne et al., 1988; Calanchi et al., 1998; Siani et al., 2004;
93 Bourne et al., 2010) and several lake settings (Magne et al., 2006; Sulpizio et al.,
94 2009; Lane et al., 2011).

95
96 Diagnostic glass chemistries for each eruption are essential in order to verify the
97 use of PP, NYT and CI in tephrostratigraphy and tephrochronology. However,
98 both the CI and NYT display chemical zoning in proximal deposits (Orsi et al.,
99 1992; 1995; Civetta et al., 1997; Pappalardo et al., 2002a). In addition, a number
100 of smaller eruptions at Phlegraean Fields also form stratigraphic markers in
101 Quaternary deposits across the Mediterranean. These smaller eruptions were fed
102 by trachyte and phonolite magmas with similar chemistries to the CI and NYT
103 products. At least twelve Pre-Campanian Ignimbrite (Pre-CI) units are recognised
104 at the Trefola Quarry (Orsi et al., 1996) spanning 59-39 ka (Pappalardo et al.,
105 1999). Several of these eruptions produced quite thick (>10 m) proximal
106 pyroclastic fall and density current deposits generated by high-energy explosive
107 eruptions from vents outside the caldera (Orsi et al., 1996). At least 20 distinct
108 tephra layers have been recognised for the same time window in the medial-
109 distal Lago Grande di Monticchio core (Wulf et al., 2007).

110
111 Between the CI and NYT eruptions, numerous surges and minor fall deposits
112 were generated from intra-caldera phreatomagmatic eruptions (Orsi et al., 1996).
113 $^{40}\text{Ar}/^{39}\text{Ar}$ dated eruptions range in age from 30.3 ka (VRa) to 14.6 ka (PRe)
114 (Pappalardo et al., 1999). These Pre-NYT units, deposited over a period of 25 ka,
115 are known collectively as Tufi Biancastri (Rittmann, 1950). Several distal tephra
116 are found in this time window. At least 10 Pre-NYT tephra layers are recorded in
117 the Lago Grande di Monticchio core, with TM-9 and TM-15 being the most
118 prominent (Wulf et al., 2004, 2007, 2008). TM-9 is linked to GM1. In distal
119 settings GM1 comprises two tephra layers closely spaced in time and is dated at
120 14.2-16.2 cal ka BP (Siani et al., 2004; Aufgebauer et al., 2012). TM-15 is
121 correlated with the 30-31 cal ka BP Y3, described in marine and terrestrial
122 settings across the central Mediterranean (Zanchetta et al., 2008).

123
124 The aims of this study using Electron Microprobe Analysis (EMPA) and Laser
125 Ablation Inductively Coupled Plasma Mass Spectrometry (LA-ICP-MS) of single
126 glass shards, are: 1) to define the diagnostic major and trace element
127 geochemistry of the PP, NYT and CI glasses and to investigate their
128 compositional heterogeneity; 2) to use these diagnostic geochemistries to
129 investigate the dispersal of the PP, NYT and CI tephra; and 3) to investigate the
130 geochemistry of pyroclastic-fall and flow deposits that predate the CI and the
131 NYT eruptions. Defining diagnostic chemistries of these Pre-CI and Pre-NYT

132 units would not only allow them to be distinguished from the CI and NYT events,
133 but also allows them to be used as stratigraphic markers.

134

135 **2. GEOLOGICAL OUTLINE**

136

137 The Phlegraean Fields lie in the Campanian Plain along the Tyrrhenian margin of
138 the southern Apennines and is part of the Quaternary potassic province. The
139 Phlegraean Fields comprises a 13 km wide nested caldera in the Gulf of Naples,
140 formed mainly as a consequence of the eruption of the CI and NYT (Orsi et al.,
141 1996). The caldera margins are poorly exposed and on the south lie beneath the
142 Bay of Pozzuoli. The Phlegraean Fields has been active since at least 60 ka
143 (Pappalardo et al., 1999) and many of the eruptions from the Phlegraean Fields
144 had large Plinian columns (>40 km) that deposited widespread fall and flow units.
145 Numerous eruptions have taken place since the NYT eruption during three
146 epochs of activity (Di Vito et al., 1999) from vents located either along the faults
147 bordering the caldera or along the extensional faults bordering the La Starza
148 resurgent block (Orsi et al., 1996). The most recent eruption produced the Monte
149 Nuovo tuff cone in 1538 AD (D'Oriano et al., 2005).

150

151 PP was a sub-Plinian to Plinian eruption, which dispersed pumice and ash mainly
152 towards the east (Lirer et al., 2001). PP was dominantly phreatomagmatic and
153 deposited alternating pumice/ash fall units and pyroclastic density currents
154 (Smith et al., 2011), which show a progressive increase in magma discharge
155 rate, as indicated by an increase in grain size and proportion of lithic fragments
156 with stratigraphic height (Lirer et al., 2001). PP magmas are tephri-phonolitic to
157 phonolitic (D'Antonio et al., 2007; Arienzo et al., 2010; Smith et al., 2011).

158

159 The NYT is the largest known trachytic phreato-Plinian eruption, extruding >40
160 km³ dense rock equivalent (DRE) of latitic-to-trachytic magma, (Orsi et al., 1992,
161 1995; Wohletz et al., 1995). Deposits of the NYT are chemically zoned and were
162 produced from three distinct magma batches, which are not related by fractional
163 crystallisation (Orsi et al., 1995). The NYT sequence is divided into a Lower
164 Member (LM) and an Upper Member (UM). The LM comprises a surge deposit
165 (LM1) produced from a central vent, overlain by an alternating sequence of
166 phreato-Plinian surge and Plinian fall deposits (LM2-LM13) all erupted from a
167 central vent (Orsi et al., 1995; Orsi et al., 1992; Wohletz et al., 1995). The UM
168 was erupted from multiple vents and deposited as pyroclastic density currents
169 following column collapse (Orsi et al., 1995; Orsi et al., 1992; Wohletz et al.,
170 1999). The poorly evolved latitic-trachitic magma dominated the end of the
171 eruption (Orsi et al., 1992; 1995; Wohletz et al., 1995) and is not recorded in the
172 precursor eruptions (Pabst et al., 2008).

173

174 The CI erupted at least 300 km³ DRE (Fedele et al., 2003) of magma during two
175 major phases. The first phase was Plinian and produced a column that reached a
176 maximum height of 44 km and deposited pumice and ash predominantly to the
177 south-east (Rosi et al., 1999). The second phase accompanied caldera collapse

178 and was characterised by highly inflated pyroclastic density currents that flowed
179 over the sea and crossed mountain ridges in excess of a thousand meters
180 (Fisher et al., 1993; Ort et al., 2003). Breccias were emplaced during the course
181 of the eruption (Fedele et al., 2008). The superposition of the variable and
182 chemically distinct pyroclastic density currents is documented in a core drilled in
183 the northern part of the city of Naples (Pappalardo et al., 2002a). On the basis of
184 the reconstruction of the CI chemical stratigraphy from the drill core, we will refer
185 to the three recognised pyroclastic density currents units as the lower,
186 intermediate and upper flow units. The explosive phases that generated these
187 units were fed by the most differentiated phonolitic magma, the compositionally
188 intermediate and the least differentiated trachytic magmas, respectively (Civetta
189 et al., 1997; Pappalardo et al., 2002a).

190
191 The CI magma chamber was compositionally zoned and is generally considered
192 to have comprised two distinct magmas (trachytic and phonolitic), which mixed
193 during the eruption (Fedele et al., 2008; Arienzo et al., 2009; Civetta et al., 1997;
194 Pappalardo et al., 2002a). There is some debate as to the relationships between
195 the trachytic and phonolitic layers. Some authors have suggested that the
196 phonolitic cap was generated by undercooling and rapid crystallisation of the
197 trachyte magma and later assimilation (Bohrson et al., 2006; Fowler et al., 2007;
198 Pappalardo et al., 2008). Fedele et al., (1008) suggest that the CI magmas in the
199 Breccia Museo formation are related by fractional crystallisation. However, the
200 least and most evolved CI end-member magmas have different Sr- and Nd-
201 isotope signatures suggesting that they evolved separately (Arienzo et al., 2009).
202 The least evolved component is seen only at the end of the CI eruption (Arienzo
203 et al., 2009; Pabst et al., 2008). This suggests late recharge of the CI chamber by
204 trachytic magma that crystallised ca. 6 ka before eruption (Arienzo et al., 2011).

205
206 The chemical heterogeneity of the CI and NYT is believed to result mostly from
207 recharge of the shallow reservoir by arrivals of less differentiated magmas and
208 mixing (Orsi et al., 1995; Pabst et al., 2008; Arienzo et al., 2009). In contrast, the
209 Pre-CI and Pre-NYT fall units each have a more restricted compositional range
210 (Pabst et al., 2008). On the basis of geochemical and isotopic data, Pabst et al.
211 (2008) argue that: 1) the Pre-CI eruptions represent distinct magma batches in
212 multiple chambers, the last of which may have provided a mixing end-member for
213 the CI, later influxed by less differentiated, less radiogenic magma; and 2) the
214 Pre-NYT magmas evolved independently from the preceding CI magmatic
215 system. The Pre-CI, CI and Pre-NYT, NYT are decoupled both geochemically
216 and isotopically and show evidence of increasing crustal contamination through
217 time since 60 ka (Di Renzo et al., 2011, D'Antonio et al., 2007; Pappalardo et al.,
218 2002b; Pabst et al., 2008; Tonarini et al., 2004).

219 220 **3. SAMPLES**

221 222 **3.1 Proximal Samples**

223

224 The ash/tephra (<2 mm) component of Plinian and co-ignimbrite clouds can be
225 dispersed by tropospheric and stratospheric systems and deposited in distal
226 localities, therefore in our proximal study we have primarily sampled thick fall and
227 flow deposits. Samples from the CI and NYT and several major Pre-CI and Pre-
228 NYT eruptions were taken from well-studied outcrops from various locations in
229 the Campanian Region (Fig. 1, Table 1). Numerous smaller eruptions recorded
230 in the stratigraphy at Trefola quarry and elsewhere are described in detail in
231 Pabst et al. (2008) and Pappalardo et al. (2002b).

232
233 The CI and NYT were both sampled at four separate localities; the Pre-CI was
234 sampled at Trefola (TL) quarry and the Pre-NYT at Trefola and Verdolino (VR)
235 quarries and at Ponti Rossi (PR). The PP samples come from Via Pigna.
236 Eruptions were sampled at various levels, except for thin deposits (<2m) where
237 only one representative sample was collected. Details of the eruptions sampled
238 and sample localities are given in Table 1. Thirty pumice/scoria clasts were
239 sampled from each level. Clasts were crushed and clean fragments from the
240 interiors of each individual clast was picked and mounted in 'Stuers EpoFix'
241 epoxy resin.

242 243 **3.2 Lago Grande di Monticchio samples**

244
245 We compare the proximal samples to distal tephra preserved within the Lago
246 Grande di Monticchio core, discussed in detail in Narcisi, (1996) and Wulf et al.
247 (2004, 2008). This lake provides an ideal distal archive for Campanian tephra
248 due to its location 120 km east of the Phlegraean Fields (Fig. 1) on the dispersal
249 axis of most eruptions (e.g. Santacroce et al., 2003). The Lago Grande di
250 Monticchio core spans 135 ka and preserves >340 distinct tephra layers, of
251 which >300 are thought to originate from the Campanian region (Wulf et al.,
252 2004). The laminated sediments of the lake provide a high-precision varve age
253 record (Wulf et al., 2008). Incremental counting error on Lago Grande di
254 Monticchio varve ages is estimated to be 5-10 % (Brandt et al., 1999; Brauer et
255 al., 2000; Wulf et al., 2008). We have determined the major and trace element
256 compositions of prominent layers from this lake that were previously correlated to
257 the PP (TM-7b), NYT (TM-8) and CI (TM-18-top and TM-18-base) and with key
258 Campanian tephra in the Pre-NYT (TM-9, TM-15) time window. Pumice and
259 glass shards from the Lago Grande di Monticchio tephra layers were picked and
260 mounted in 'Stuers EpoFix' epoxy resin for analysis.

261 262 **4. ANALYTICAL METHODS**

263 264 **4.1 Electron Micro-Probe Analysis**

265
266 Major element compositions were determined using Jeol8600 electron
267 microprobe, equipped with 4 wavelength dispersive spectrometers and SamX
268 software, at the Research Laboratory for Archaeology and the History of Art,
269 University of Oxford. An accelerating voltage of 15 kV, low beam current (6 nA),

270 and defocused (10 μm) beam were used to minimize Na migration. Count times
271 were 30 s, except for Na (10 s) and P and Cl (each 60 s). The instrument was
272 calibrated using a suite of appropriate mineral standards. The calibration was
273 verified using a range of secondary glass standards from the Max Planck
274 Institute, Leipzig, Germany. Secondary glass (MPI-DING suite; Jochum et al.,
275 2006) and mineral (Smithsonian Institute; Jarosewich, 2002) standards were
276 analysed between and within runs. The PAP absorption correction method was
277 used. Three replicate analyses were made on each sample and analyses with
278 totals of <95 % were discarded. Sample totals are normalised to 100 wt% in all
279 plots and tables. Accuracies of analyses of the MPI-DING glasses are <5 % for
280 concentrations >0.8 wt%; concentrations <0.2 wt% are more qualitative.
281 Analytical precision is <10 % relative standard deviation (%RSD) for analytes
282 with concentrations >0.8 wt%. Error bars on plots show 2 s.d. of replicate
283 analyses of StHs6/80-G and ATHO-G.

284

285 **4.2 Laser Ablation Inductively Coupled Plasma Mass Spectrometry**

286

287 LA-ICP-MS analyses of proximal tephra samples were performed using an
288 Agilent 7500ce coupled to a Resonetics 193 nm ArF excimer laser-ablation
289 system (RESOLUTION M-50 prototype) with a two-volume ablation cell (Müller et
290 al., 2009) at the Department of Earth Sciences, Royal Holloway University of
291 London. We used 57, 34 and 25 μm laser spots, depending on the size of the
292 area available for analysis in individual samples. The repetition rate was 5 Hz
293 and the count time was 40 s (200 pulses) on the sample and 40 s on the gas
294 blank (background). Concentrations were calibrated using NIST612 with ^{29}Si as
295 the internal standard. Data reduction was performed manually using Microsoft
296 Excel allowing removal of portions of the signal compromised by the occurrence
297 of microcrysts, full details of the analytical and data reduction methods are given
298 in Tomlinson et al. (2010). Accuracies of analyses of ATHO-G and StHs6/80-G
299 MPI-DING glass analyses are typically <5 %. Reproducibility of ATHO-G
300 analyses is <5 RSD% for all trace elements except for V (ATHO-G) and Gd
301 (StHs6/80-G), which are close to LOD. Relative standard errors (%RSE) for
302 sample tephra analyses are typically <2 %RSE for V, Rb, Y, Zr, Nb, La, Ce, Pr,
303 Th, U; and <5% for Ti, Sr, Ba, Nd, Sm, Eu, Gd, <Dy, Er, Yb, Lu and Ta. Full
304 errors (standard deviations and standard errors for individual sample analyses)
305 are given in the supplementary information. For consistency with EMPA error
306 reporting, error bars on plots show 2 s.d. of replicate analyses of StHs6/80-G and
307 ATHO-G.

308

309 **5. RESULTS**

310

311 Representative major and trace element compositions of proximal pumice
312 glasses are given in Tables 2 and 3 and of distal Lago Grande di Monticchio
313 glass shards in Table 4. The full dataset is available as supplementary data. In
314 this section we will highlight aspects of the chemistry that allow us to distinguish
315 between the eruptive units, thus revealing the chemical features that can be used

316 in proximal-distal correlations. Diagnostic ratios are summarised in Table 5.
317 Eruptive units are described in order of increasing age consistent with the order
318 of occurrence of tephra with increasing depth in sedimentary records.

319

320 **5.1 PP**

321

322 The PP glasses are phonolitic (56.58-58.71 wt% SiO₂) and extend into the tephri-
323 phonolite field (Fig. 2) with increasing stratigraphic height. There is a negative
324 relationship between SiO₂ and CaO, MgO, FeO and TiO₂; K₂O (7.9-9.3 wt%)
325 slightly increases with increasing SiO₂, while Al₂O₃ (18.5-19.5 wt%), MnO (0.1-
326 0.2 wt%) and Na₂O (3.3-3.9 wt%) remain approximately constant (Fig. 3a-f). PP
327 glasses have a low degree of evolution (Zr/Sr = 0.27-0.36 and Eu/Eu*_N = 0.65-
328 0.94) and are characterised by relatively low Th concentrations (20-29 ppm) with
329 constant ratios of HFSE to Th (Nb/Th = 1.75 ± 0.15; Zr/Th = 10.5 ± 0.5; Y/Th =
330 1.0 ± 0.1; Ta/Th = 0.08 ± 0.01) and high V concentrations (94-132 ppm) (Fig. 4a-
331 f).

332

333 PP glasses overlap extensively with the low SiO₂ component of the NYT- LM and
334 -UM glasses (section 4.2), but have lower MgO (and to a lesser extent FeO) for a
335 given SiO₂ content (Fig. 3a-f). Therefore, the PP and NYT units can be
336 distinguished using major element compositions.

337

338 **5.2 NYT-series (NYT, Pre-NYT)**

339

340 Pre-NYT and NYT glasses show a negative relationship between SiO₂ and CaO,
341 MgO, FeO and TiO₂; K₂O and Na₂O show an inflection at ~60 wt% SiO₂ with
342 Na₂O increasing and K₂O decreasing at higher SiO₂; Al₂O₃ stays approximately
343 constant (Fig. 3a-f). Chlorine is positively correlated with Na₂O. The Pre-NYT
344 units form clusters at the most and least evolved ends of the array, while the NYT
345 itself spans the whole compositional range. The NYT-series glasses have
346 constant ratios of HFSE to Th: Nb/Th = 1.7 ± 0.1; Zr/Th = 10.9 ± 0.6; Ta/Th =
347 0.08 ± 0.01. They show low degrees of evolution (Fig. 4b): Eu/Eu*_N = 0.3-1.0, the
348 largest being observed in the Pre-NYT unit TLo; Zr/Sr = 0.2-7 in most NYT-series
349 units and 30-59 in TLo (Fig. 5f). The NYT-series has high V concentrations (20-
350 170 ppm, Fig. 5e).

351

352 *5.2.1 NYT*

353

354 Glasses from analysed NYT-LM units (LM1, LM3, LM13) form two clusters
355 separated by a distinct compositional gap (LM3 and LM13 both have >3.8 wt%
356 CaO, <59 wt% SiO₂; LM1 has <2.6 wt% CaO and >61 wt% SiO₂). The LM1 glass
357 is a trachyte (Fig. 2), and not strongly evolved (Sr/Zr = 0.4-1.8) with weak
358 anomalies relating to feldspar fractionation (Eu/Eu*_N = 0.6-0.9; Sr/Pr_N = 0.8-1.2).
359 The LM3 and LM13 glasses are phono-trachytes (Fig. 2) and also only weakly
360 evolved (Sr/Zr = 0.3-0.4) but with higher incompatible element concentrations
361 and larger Eu and Sr anomalies (Eu/Eu*_N = 0.6-0.8; Sr/Pr_N = 0.7-0.9) than LM1.

362 These two clusters represent magma 1 and magma 2 described by Orsi (1995).
363 Glass shards of less differentiated composition (latite to trachyte), corresponding
364 to magma 3 of Orsi et al. (1995), are not seen in this study.

365
366 Glasses from the units of the UM straddle the phonolite-trachyte boundary and
367 span a wide compositional range between the two LM clusters and extend to less
368 evolved compositions, with 56.0–62.1 wt% SiO₂ and 2.0–5.1 wt% CaO (Fig. 3)
369 and Zr/Sr = 0.2–7.3.

370
371 In summary, NYT glasses are characterised by the following compositional
372 features:

- 373 1. Straddle the phono-trachyte boundary at 56.0–62.1 wt% SiO₂.
- 374 2. The analysed LM units are bimodal with a trachytic component (<2.6 wt%
375 CaO and >61 wt% SiO₂) and a phono-trachytic component (>3.8 wt%
376 CaO, <59 wt% SiO₂).
- 377 3. The UM forms a continuum which overlaps with the two LM clusters and
378 extends to less differentiated compositions.

379 380 5.2.2 Pre-NYT

381
382 The Pre-NYT units are collectively known as Tufi Biancastri (Rittmann, 1950),
383 however they represent the products of several eruptions. Here we have
384 analysed four Pre-NYT units, these are (youngest to oldest): PRa (16.1 ± 0.2
385 ⁴⁰Ar/³⁹Ar ka; Pappalardo et al., 1999), VRb, VRa (30.3 ± 0.2 ⁴⁰Ar/³⁹Ar ka;
386 Pappalardo et al., 1999) and TLo. The PRa, VRb and TLo units have restricted
387 compositional ranges, while the VRa forms two clusters.

388
389 Glasses from the Pre-NYT PRa are trachytic (Fig. 2) with 62.4 ± 0.5 wt% SiO₂,
390 and 2.2 ± 0.3 wt% CaO. They are moderately enriched in trace elements (Sr/Zr =
391 1.3 ± 0.4; Eu/Eu*_N = 0.68 ± 0.07; Sr/Pr_N = 0.23 ± 0.09) and overlap with the
392 trachytic NYT, LM1 glasses.

393
394 Glasses from Pre-NYT VRb are trachytic (Fig. 2) with 62.2 ± 0.4 wt% SiO₂ and
395 2.2 ± 0.2 wt% CaO. In terms of trace elements, the VRb glasses are moderately
396 enriched (Sr/Zr = 1.7 ± 1.2; Fig. 5) and largely overlap with the PRa glasses, but
397 show a slightly wider compositional range extending to slightly higher HFSE
398 concentrations and slightly larger feldspar related anomalies (Eu/Eu*_N = 0.6 ±
399 0.1; Sr/Pr_N = 0.20 ± 0.14; Fig. 4). Glasses from unit VRb also overlap with the
400 trachytic NYT-LM1.

401
402 Glasses from the Pre-NYT VRa are bimodal (Fig. 2–5). One population is
403 trachytic (62.3 ± 0.4 wt% SiO₂, 2.2 ± 0.1 wt% CaO) with moderate enrichment
404 levels and Eu and Sr anomalies (Sr/Zr = 1.4 ± 1.0; Eu/Eu*_N = 0.70 ± 0.15; Sr/Pr_N
405 = 0.25 ± 0.14). This cluster overlaps with trachytic NYT-LM1. The second
406 population is phono-trachytic (58.0 ± 0.5 wt% SiO₂, 4.0 ± 0.3 wt% CaO), is
407 weakly enriched (Sr/Zr = 0.34 ± 0.02; Fig. 5) and has small feldspar related

408 anomalies ($\text{Eu}/\text{Eu}^*_\text{N} = 0.81 \pm 0.04$; $\text{Sr}/\text{Pr}_\text{N} = 0.86 \pm 0.04$; Fig 4). This cluster
409 overlaps with the phono-trachytic NYT-LM (LM3 + LM13), but extends to slightly
410 higher FeO and MgO for a given SiO_2 concentration, and has slightly lower Sr
411 and Ba concentrations relative to the NYT.

412
413 Glasses from the Pre-NYT unit TLo are trachytic (Fig. 2) with 1.5 ± 0.1 wt% CaO
414 and the highest SiO_2 and Na_2O among the studied Pre-NYT units (63.9 ± 0.4
415 wt% SiO_2 and 6.0 ± 0.3 wt% Na_2O , respectively). The TLo glasses differ from
416 those of the other NYT-series units, they are highly evolved ($\text{Sr}/\text{Zr} = 30\text{-}59$), have
417 larger feldspar related anomalies ($\text{Eu}/\text{Eu}^*_\text{N} = 0.32 \pm 0.04$, $\text{Sr}/\text{Pr}_\text{N} = 0.011 \pm 0.04$)
418 and contain higher concentrations of other incompatible elements (Fig 4, 5). The
419 TLo can be distinguished from the NYT on the basis that it has significantly
420 higher HFSE and Th concentrations (Fig 5a,b).

421

422 In summary:

- 423 1. It is extremely difficult to distinguish products of the Pre-NYT eruptions
424 from the NYT using major and trace element geochemistry.
- 425 2. The trachytic component of the NYT-LM1 overlaps with the Pre-NYT units
426 PRa, VRb and the trachytic population of VRa.
- 427 3. The phono-trachytic component of the NYT-LM (LM3 and LM13) overlaps
428 with the phono-trachytic component of Pre-NYT unit VRa.
- 429 4. VRa is distinctive among the studied Pre-NYT eruptions as it is bimodal. It
430 can be distinguished from the other studied Pre-NYT units on the basis of
431 slightly higher MgO and FeO and lower Ba and Sr.
- 432 5. Glasses from the Pre-NYT units have slightly lower V concentrations than
433 those from the NYT deposits.
- 434 6. The compositional overlap within the Pre-NYT coupled with the number of
435 Pre-NYT units, mean that it is difficult to distinguish between the Pre-NYT
436 eruptions.
- 437 7. TLo is clearly distinguished from the other Pre-NYT units studied herein,
438 but indicates the occurrence of more evolved Pre-NYT magmas.

439

440 **5.3 CI-series (CI, Pre-CI)**

441

442 Pre-CI and CI glasses have a narrow range of CaO, MgO, FeO, TiO_2 (1.3-2.2,
443 0.26-0.52, 2.4-3.5 and 0.34-0.46 wt%, respectively) for a wide range of SiO_2
444 contents (55-63 wt%) (Fig. 3). Concentrations of SiO_2 , Al_2O_3 and K_2O are
445 clustered within the Pre-CI units and the CI fall deposits. Within these units, K_2O
446 and Al_2O_3 decrease with increasing SiO_2 ; this trend continues in a stepwise
447 manner through the studied Pre-CI units to the CI. Chlorine and Na_2O are also
448 clustered and show a positive correlation, but are slightly higher in the Pre-CI
449 samples relative to CI. In contrast to the Pre-CI units and the CI fall, glasses from
450 the CI lower and intermediate flows have a wider range of SiO_2 contents and
451 SiO_2 is positively correlated with Al_2O_3 and K_2O . Geochemical variation within the
452 CI is consistent with mixing between the evolved CI magma (erupted as both fall
453 and the lower and intermediate flows) and a less evolved magma (Civetta et al.,

1997; Arienzo et al., 2009). The CI upper flow, which was deposited at the end of the eruption, is less evolved and isotopically distinct from the rest of the CI-series (Arienzo et al., 2009).

Incompatible element concentrations define positive linear correlations within the CI-series (Fig. 5), except for those elements that are depleted during feldspar fractionation (Eu, Sr, Ba). Ratios of HFSE to Th are constant within the CI-series glasses ($\text{Nb/Th} = 2.4 \pm 0.3$; $\text{Zr/Th} = 13 \pm 1$; $\text{Ta/Th} = 0.11 \pm 0.01$). Relative to the NYT-series, the CI-series has a higher Th concentration, higher HFSE contents, higher ratios of HFSE to Th, and low V concentrations (11-26 ppm). The CI-series also has larger Eu anomalies ($\text{Eu/Eu}^*_\text{N} = 0.2-0.5$) than in the NYT series. The higher degree of evolution of the CI-series can also be seen in the ratio $\text{Zr/Sr} = 5-84$ (Fig. 5f).

467

5.3.1 CI

469

Glasses from the CI fall and from the lower and intermediate flow units straddle the trachyte-phonolite boundary and overlap extensively in major element composition (Fig. 2,3). In terms of trace elements, the fall is compositionally intermediate to evolved, with $\text{Zr/Sr} = 5-31$ (Fig. 5f) and shows negative anomalies in Sr ($\text{Sr/Pr}_\text{N} = 0.01-0.08$) and Eu ($\text{Eu/Eu}^*_\text{N} = 0.24-0.34$) consistent with feldspar fractionation (Fig. 4c). Glasses from the lower and intermediate flow units overlap widely with those from the fall and are also compositionally intermediate to evolved in composition, with $\text{Zr/Sr} = 8-28$. However, glasses from the lower and intermediate flows lack the most enriched compositions present in the CI fall and feldspar related anomalies are not so prominent ($\text{Sr/Pr}_\text{N} = 0.01-0.04$; $\text{Eu/Eu}^*_\text{N} = 0.27-0.36$). Concentrations of incompatible elements that are not affected by feldspar fractionation are typically lower in glasses from the lower and intermediate flows (Th = 41-51, Ba = 15-65; Nb = 13-117) than in the fall (Th = 41-62; Ba = 13-105; Nb = 13-136) components of the CI. The fall and flow (lower and intermediate) can be most clearly distinguished on a plot of Zr-Th (Fig. 6).

485

The magma feeding the CI upper flow unit is distinctive from the magma feeding the underlying fall and flows, as it is a trachyte (Fig. 2). The CI upper flow glasses have higher concentrations of CaO, MgO, K₂O (2.5, 0.76 and 8.1 wt%, respectively) and V (<64 ppm), and lower Na₂O (2.8-4.9 wt%) than the CI fall and lower/intermediate flows (Fig. 3, 5). They have ratios of Na₂O/K₂O <0.6. The analysed glasses extend to poorly evolved compositions with $\text{Zr/Sr} = 0.4$ and negligible Eu and Sr anomalies ($\text{Eu/Eu}^*_\text{N} = 1.1$; $\text{Sr/Pr}_\text{N} = 0.7$). Ratios of HFSE to Th are higher than for the glasses from the CI fall and lower and intermediate flows and are transitional, with more evolved samples plotting close to the CI fall and lower/intermediate flow compositions and a less evolved magma composition.

497

In summary, the CI analysed glasses are characterised by the following features:

- 499 1. Glasses from the fall and the lower and intermediate flows straddle the
500 phono-trachyte boundary and those from the upper flow are trachytic in
501 composition (e.g. Arienzo et al., 2009; Civetta et al., 1997; Pappalardo et
502 al., 2002a).
- 503 2. Glasses from the fall and the lower and intermediate flows have
504 overlapping compositions and show a continuous range from intermediate
505 to evolved compositions, with the flows extending to less evolved
506 compositions. They can be separated on a plot of Zr-Th.
- 507 3. Glasses from the upper flow span a range between the CI fall and a less
508 differentiated end-member composition and have $\text{Na}_2\text{O}/\text{K}_2\text{O} < 0.6$.

510 5.3.2 Pre-CI

511
512 Pre-CI units (youngest to oldest) Tlf, TLc and TLa (58 ± 3 $^{40}\text{Ar}/^{39}\text{Ar}$ ka;
513 Pappalardo et al., 1999) all have narrow compositional ranges in both major and
514 trace elements (Fig. 3, 5), as previously shown by Pabst et al. (2008) on the
515 basis of whole rock compositions. Glasses from the Pre-CI units are phonolitic
516 (Fig. 2) and are distinct from CI eruption glasses in terms of major element
517 composition. The Pre-CI units are characterised by low SiO_2 and high CaO, FeO
518 and Al_2O_3 concentrations relative to the CI. In addition, Na_2O is higher in the Pre-
519 CI units than in the fall and flows of the CI. The incompatible elements
520 enrichment in the Pre-CI units decreases in the order $\text{TLa} > \text{TLc} > \text{Tlf}$ (Fig. 4d).

521
522 The Tlf is the last large unit deposited prior to the eruption of the CI. Relative to
523 the other Pre-CI units analysed, the Tlf glasses have higher MgO contents and
524 higher K_2O and higher but overlapping SiO_2 and have lower Na_2O and lower but
525 overlapping FeO (Fig 3). In terms of trace element composition, Tlf glasses are
526 moderately evolved ($\text{Zr}/\text{Sr} = 8\text{-}22$) and have a smaller Eu anomaly ($\text{Eu}/\text{Eu}^*_\text{N} =$
527 0.45 ± 0.06) and lower Th and HFSE element concentrations than TLa and TLc.
528 Tlf overlaps with the CI evolved component in terms of incompatible element
529 composition, but differs in major elements.

530
531 The TLc glasses have the lowest SiO_2 content of the Pre-CI units analysed (58.6
532 ± 0.4 wt%). They are compositionally moderately evolved with moderate feldspar
533 related anomalies ($\text{Zr}/\text{Sr} = 41\text{-}58$, $\text{Eu}/\text{Eu}^*_\text{N} = 0.31 \pm 0.03$). The TLc glasses
534 overlap strongly with TLa glasses in both major and trace element composition
535 (Fig. 3, 5), the main differences being that TLc glasses have higher Al_2O_3 ($19.8 \pm$
536 0.3 wt%), higher but overlapping Th and lower but overlapping ratios of HFSE to
537 Ti ($\text{Zr}/\text{Ti} = 0.32 \pm 0.02$; $\text{Nb}/\text{Ti} = 0.063 \pm 0.003$; $\text{Y}/\text{Ti} = 0.025 \pm 0.001$).

538
539 The TLa glasses are intermediate between TLc and Tlf for all major elements
540 except that it has lower Al_2O_3 (19.6 ± 0.3 wt%). The TLa glasses show a similar
541 degree of chemical evolution to TLc ($\text{Zr}/\text{Sr} = 17\text{-}56$, $\text{Eu}/\text{Eu}^*_\text{N} = 0.33 \pm 0.06$),
542 except for lower Al_2O_3 (19.6 ± 0.3 wt%) and higher but overlapping ratios of
543 HFSE to Ti ($\text{Zr}/\text{Ti} = 0.34 \pm 0.01$; $\text{Nb}/\text{Ti} = 0.066 \pm 0.004$; $\text{Y}/\text{Ti} = 0.027 \pm 0.001$).

544

545 In summary:

- 546 1. The Pre-CI units TLa, TLc and Tlf are clearly distinguished from the CI on
547 the basis that they are phonolitic, while the CI is phonolite-trachyte and
548 have lower SiO₂ and higher CaO, FeO and Al₂O₃ concentrations.
- 549 2. The Pre-CI units TLa and TLc are similar in major and trace element
550 composition but can be distinguished from each other on the basis of
551 SiO₂, Al₂O₃, Th and ratios of HFSE to Ti.
- 552 3. The Pre-CI unit Tlf is distinct from TLa and TLc, it has lower Th, Nb, Y, Zr,
553 and larger Eu anomalies
- 554 4. The possible presence of other Pre-CI units in distal locations means that
555 it may be difficult to confidently distinguish between Pre-CI units.

556

557 **5.4 Comparing the NYT- and CI-series**

558

559 The CI-series (60-39 ka) and the NYT-series/PP (39-12 ka) can be distinguished
560 using both major and trace element compositions. The most diagnostic criteria
561 are:

562

- 563 1. The NYT-series have higher ratios of CaO/SiO₂, MgO/SiO₂ and TiO₂/SiO₂
564 and lower Al₂O₃/SiO₂ ratios and lower Na₂O, Cl and MnO concentrations
565 relative to the CI-series.
- 566 2. Ratios of HFSE to Th distinguish members of the NYT-series (Nb/Th = 1.7
567 ± 0.1; Zr/Th = 10.9 ± 0.6; Ta/Th = 0.08 ± 0.01) and the CI-series (Nb/Th =
568 2.4 ± 0.3; Zr/Th = 13 ± 1; Ta/Th = 0.11 ± 0.01).
- 569 3. The CI-series (Zr/Sr = 5-84) is significantly more evolved than the NYT-
570 series (Zr/Sr = 0.2-7).
- 571 4. Feldspar fractionation signatures are typically larger in the CI-series
572 (Eu/Eu*_N = 0.2-0.5) than the NYT-series (Eu/Eu*_N = 0.3-1.0).
- 573 5. Vanadium concentrations are higher in the NYT-series (20-170 ppm)
574 relative to the CI-series (11-26 ppm).

575

576 The NYT-series and CI-series trends appear to converge at the least evolved
577 compositions (low incompatible element concentrations) on trace element plots
578 (Fig.5a-d). Glass compositions from the CI upper flow extend between the CI fall
579 and a composition similar to the least evolved NYT-series magma. Ratios of
580 HFSE to Th in the CI upper flow are lower than for the rest of the CI-series (Table
581 5) and are also transitional between the CI- and NYT-series.

582

583 **6. DISCUSSION**

584

585 **6.1 Proximal-distal correlation with Lago Grande di Monticchio tephra**

586

587 In the following sections, we compare the proximal data to new major and trace
588 element data for tephra in the medial-distal Lago Grande di Monticchio archive
589 (Table 4). We use the diagnostic geochemistries defined proximally and, in some
590 cases at Lago Grande di Monticchio, to assess distal occurrences of Phlegraean

591 Fields tephra in the literature. This allows an improved understanding of the
592 dispersal of tephra from PP, NYT and CI. A summary of tephra dispersal
593 characteristics is given in table 6.

594

595 *6.1.1 Pomici Principali (PP) & C-1/TM-7b*

596

597 Major and trace element analyses indicate that the PP can be distinguished from
598 the NYT-series tephras on the basis of lower MgO and FeO for a given SiO₂
599 concentration (Fig 3b,c). Trace element compositions of the PP and NYT-series
600 overlap widely (Fig. 4a).

601

602 The PP is correlated with TM-7b in Lago Grande di Monticchio (Narcisi, 1996;
603 Wulf et al., 2004; Smith et al., 2011). Major and trace element data for TM-7b
604 glasses is given in table 4. TM-7b glasses show a good match with PP for all
605 trace element ratios, including HFSE/Th and elements affected by plagioclase
606 crystallisation (Sr, Ba, Eu) supporting a proximal-distal correlation (Fig.6a). The
607 TM-7b glass analyses span a narrower compositional range than the PP glasses
608 sampled at Via Pigna (Fig. 3-5, 7a).

609

610 The PP has been linked to tephra C-1 in marine cores from the South Adriatic
611 (Paterne et al., 1988; Siani et al., 2004; Calanchi et al., 2008). The tephra
612 compositions reported by Siani et al. (2004) and Calanchi et al. (2008) overlap
613 with the proximal datasets reported herein and in Smith et al. (2010) and with
614 Lago Grande di Monticchio tephra TM-7b (Fig. 8a). The C-1 tephra of Paterne et
615 al. (1988) is more evolved than the proximal samples, but lies on the PP trend
616 with respect to MgO-SiO₂ (Fig. 8a) and is considered to have been sourced from
617 the PP eruption. In contrast, reported occurrences of C-1/PP tephra in the central
618 Adriatic (Bourne et al., 2010; Calanchi et al., 2008) do not correlate with the
619 proximal PP reported here or by Smith et al. (2010). Bourne et al. (2010) report a
620 cryptotephra layer from a central Adriatic core which comprises tephra from both
621 the NYT and PP eruptions, however the reported data all lie on the higher MgO-
622 SiO₂ trend of the NYT, Bourne (2012) later correlated this layer with TM-8, rather
623 than TM-7b on the basis of further data. Calanchi et al. (2008) report a tephra in
624 a central Adriatic core, whose geochemistry differs significantly from the proximal
625 PP and TM-7b. The authors linked this tephra to PP on the basis that it is
626 comparable to TM-7a, however this LGM tephra does not have a PP chemistry
627 (Wulf et al., 2004). The composition of TM-7a overlaps with the NYT-series in
628 MgO-SiO₂. PP is not documented in any Tyrrhenian Sea cores in the study of
629 Paterne et al. (1988). Therefore, we suggest that the PP has not yet been found
630 in the central Adriatic and marine occurrences of the PP are currently confined to
631 the south Adriatic.

632

633 The PP tephra has also been reported in terrestrial cores, Lake Bled (Slovenia,
634 Lane et al., 2011), Lake Shkodra (Albania and Montenegro, Sulpizio et al., 2010)
635 and Lake Accesa (Italy, Mangy et al., 2006). In Lake Bled, 620 km north of
636 Phlegraean Fields, a cryptotephra correlated to PP shows a good overlap with

637 the proximal data reported here and extends to more evolved compositions
638 (Fig.7a), suggesting that the PP magma spans a wider compositional range than
639 is represented proximally. The reported mean composition of the Lake Shkodra
640 tephra, from a location 440 km east of the Phlegraean Fields, does not lie on the
641 PP compositional trend and appears more similar to the NYT-series glasses
642 reported herein. The age of the layer at lake Shkodra is poorly constrained
643 (Sulpizio et al., 2010). Finally, Magny et al. (2006) report two distinct tephra
644 layers with characteristics similar to the PP tephra in a core from Lake Accesa,
645 Italy, but neither PP1 nor PP2 is comparable to the proximal PP glass
646 compositions.

647
648 This re-examination of distal occurrences of the PP suggests that the areal extent
649 of this tephra is limited. The presence of PP tephra in the south Adriatic and
650 absence in the central Adriatic indicates that the PP was dominantly distributed to
651 the east. However, the occurrence of cryptotephra in Lake Bled indicates some
652 dispersal to the north. Distal settings appear to preserve more evolved
653 compositions than are known from the proximal deposits.

654 655 *6.1.2 The Neapolitan Yellow Tuff (NYT) & C-2/TM-8*

656
657 Major and trace element analyses of proximal glasses indicate that the NYT
658 tephra may be distinguished from the trachytic, geochemically similar Pre-NYT
659 tephra, on the basis of the occurrence of less evolved phono-trachytic
660 compositions, either representing the less differentiated cluster at 57.5-58.5 wt%
661 SiO₂ (NYT-LM) and/or the less differentiated portion (down to 56.0 wt% SiO₂) of
662 the continuous trend (NYT-UM). The Pre-NYT VRa layer is also bimodal with a
663 phono-trachytic component, but the NYT is separated on the basis of lower CaO
664 and FeO (Fig. 3a,c) and higher Ba and Sr. In the following section we assess
665 previously correlated occurrences of the NYT tephra in terms of the dispersal of
666 the LM and UM components.

667
668 The NYT has been correlated with the Lago Grande di Monticchio tephra TM-8
669 (Wulf et al., 2004). The TM-8 glasses (Table 4) have two modes (61.5-62 wt%
670 SiO₂ and 56.0-58.4 wt% SiO₂). The high-SiO₂ TM-8 glasses show a good match
671 to the high-SiO₂ cluster in the NYT-LM, while low-SiO₂ TM-8 glasses overlap with
672 the low-SiO₂ cluster in the NYT-LM. The TM-8 glass compositions extend to less
673 evolved, tephra-phonolitic compositions (lower SiO₂, K₂O, Na₂O and higher FeO,
674 MgO and CaO; Fig. 3) with higher Ba and Sr concentrations and lower Zr/Sr
675 ratios (Fig. 5) consistent with the NYT-UM and there are some shards of
676 intermediate composition (58-61 wt% SiO₂), which are also associated with the
677 NYT-UM. Therefore, both phases of the NYT eruption are recorded at Lago
678 Grande di Monticchio (Fig. 7b,c).

679
680 The NYT has been correlated to marine tephra C-2 in distal settings up to 250 km
681 from the Phlegraean Fields in the Tyrrhenian and Adriatic Seas (Paterne et al.,
682 1988; Bourne et al., 2010; Calanchi et al., 1998; Siani et al., 2004). C-2 is dated

683 at 13.84-14.88 cal ka BP in Adriatic core MD90-917. In each of the Tyrrhenian
684 and Adriatic marine cores, the C-2 layer is characterised by the presence of low-
685 silica glasses (<57.5 wt% SiO₂) and by a differentiation trend from phono-
686 trachytic, low-SiO₂ to phonolitic, high-SiO₂ compositions (Paterne et al., 1988;
687 Bourne et al., 2010; Calanchi et al., 1998; Siani et al., 2004). This is consistent
688 with a correlation to the NYT rather than any of the geochemically similar Pre-
689 NYT layers. Specifically, distal occurrences of NYT tephra in the Tyrrhenian Sea
690 to the west and south-west of Phlegraean Fields and the Adriatic Sea to the east
691 and north-east of Phlegraean Fields may record both the NYT-LM and NYT-UM
692 (Fig.7b). This is clear in the PRAD218 central Adriatic core (Bourne et al., 2010)
693 because compositional data is given for individual glass shards, allowing both the
694 NYT-UM trend and the NYT-LM low- and high SiO₂ clusters to be seen. The C-2
695 tephra data of Paterne (1988), Calanchi et al., (1998) and Siani et al., (2004)
696 appear to be dominated by the NYT-UM, but this is not clear because only mean
697 tephra compositions are given, masking the compositional range and possibly the
698 actual magma composition.

699
700 The NYT tephra has been identified in terrestrial cores from Lake Bled (Slovenia,
701 Lane et al., 2011) and Längsee, Austria (Schmidt et al., 2002), approximately 620
702 and 650 km north of Phlegraean Fields, respectively. The correlated tephra
703 layers are bimodal, with clusters overlapping the phono-trachytic and trachytic
704 populations in the NYT-LM (Fig.7b).

705
706 Both the bimodal NYT-LM and the continuous NYT-UM occur in distal localities.
707 The NYT-UM is expected to form thicker tephra layers on the basis of its larger
708 relative volume. The NYT-UM is the dominant NYT tephra in settings to the east
709 and west of the Phlegraean Fields. However, the NYT-LM is found in the
710 absence of the NYT-UM in locations (to date) up to 650 km north of the
711 Phlegraean Fields.

712 713 6.1.3 Pre-NYT

714
715 Numerous eruptions punctuate the time period between the CI and NYT events,
716 five are recorded at Trefola and Verdolino, and nine at Ponti Rossi (Orsi et al.,
717 1996). We have analysed four of these Pre-NYT units, the data indicates that this
718 phase of Phlegraean Fields activity is characterised by repeated eruption of very
719 similar trachytic magmas. Tephra from the Pre-NYT eruptions may be widely
720 dispersed, at least 10 Pre-NYT tephra layers are recorded in the Lago Grande di
721 Monticchio core, with TM-9 and TM-15 being the most prominent (Wulf et al.,
722 2004; 2007; 2008). Several important distal tephra layers correlated with
723 Phlegraean Fields fall in the Pre-NYT/Tufi Biancastri time window, including
724 GM1, Lagno Amendolare and Y-3. Siani et al. (2004) propose that some
725 previously recognised occurrences of the C-2 tephra layer (NYT) may correlate
726 with GM1, or may contain more than a single tephra, because the close
727 chronology of these events makes them difficult to distinguish stratigraphically.

728

729 6.1.3.1 *TM-9/GM1* has previously been linked (Wulf et al., 2004) to the youngest
730 of the Tufi Biancastri deposits, Ponti Rossi unit PRe dated at 14.6 ± 0.4 $^{40}\text{Ar}/^{39}\text{Ar}$
731 ka (Pappalardo et al., 1999), which was not analysed in this study.

732
733 The TM-9 is a 2 cm thick tephra layer with a varve age of 14.56 ka BP from Lago
734 Grande di Monticchio (Wulf et al., 2004, 2008). New major and trace element
735 data for TM-9 glasses are given in Table 4. The major (FeO/CaO) and trace
736 (HFSE/Th: Fig. 5) element ratios of TM-9 glasses are consistent with the NYT
737 series. Like the proximal Pre-NYT units studied here, the TM-9 glass displays a
738 narrow range of major (1.85-1.99 wt% CaO, 62.1-63.1 wt% SiO₂) and trace
739 element compositions. However, TM-9 has higher incompatible trace element
740 concentrations (HFSE and Th) and lower V, Ba and Sr concentrations than any
741 of the similar proximal Pre-NYT products studied here (Fig. 3, 5). When
742 compared to whole rock data for proximal unit PRe (Pappalardo et al., 1999),
743 TM-9 appears to be similar, and lower SiO₂, Na₂O, Rb and Nb and higher FeO,
744 K₂O, V and Ba may be within error given the differing analytical techniques,
745 however glass geochemical data is required to fully assess the TM-9 – PRe
746 correlation suggested by Wulf et al. (2004).

747
748 TM-9 has been linked to GM1 (Wulf et al. 2004). GM1 is thought to be sourced
749 from the Phlegraean fields, but its type locality is a layer on the slopes of
750 Somma-Vesuvius, where it occurs stratigraphically above the Lagno Amendolare
751 deposits (Andronico et al., 1996; Zanchetta et al., 2000). Tephra layers correlated
752 to GM1 are described from the Adriatic Sea, where two layers (14.7 and 15.5 cal
753 ka BP) are found below the C-2/NYT layer (Siani et al., 2004), and from Lake
754 Prespa, Albania where two layers are also described (Aufgebauer et al., 2012).
755 Our data from TM-9 reveals higher Na₂O and lower K₂O relative to published
756 compositions of the GM1 type-site and distal GM1 tephra (Fig.7c,d), therefore we
757 suggest that TM-9 and GM1 may not represent the same Pre-NYT event.

758
759 6.1.3.2 *Lagno Amendolare/TM-10* The type-site for Lagno Amendolare is an
760 outcrop on the northern flank of Vesuvius, and is characterized by a mix of light
761 and dark coloured pumice and dated at 15.2-16.5 cal ka BP (Andronico et al.,
762 1996). A tephra that is correlated to TM-10 is described in the Adriatic Sea (Siani
763 et al., 2004; Bourne et al., 2010) where it is dated at 16.1-16.9 cal ka BP (Siani et
764 al., 2004). This layer was not analysed in this study and is not discussed here.

765
766 6.1.3.3 *Y-3/TM-15* has previously been linked (Wulf et al., 2004) to the Pre-NYT
767 Tufi Biancastri unit VRa (Di Vito et al., 2008) sampled in this study and dated at
768 30.3 ± 0.2 $^{40}\text{Ar}/^{39}\text{Ar}$ ka (Pappalardo et al., 1999).

769
770 TM-15 is a 29 cm thick tephra layer with a varve age of 27.26 ka BP from Lago
771 Grande di Monticchio. New major and trace element data for TM-15 glasses are
772 given in Table 4. The major (FeO/CaO) and trace (HFSE/Th) element ratios of
773 TM-15 glasses (Table 4) are consistent with the Pre-NYT series. TM-15 glasses
774 have higher MgO and FeO for a given SiO₂ (Fig. 3), consistent with VRa and

775 partially overlap with the trachytic component of the bimodal VRa (the lower part
776 of the proximal sequence). However, TM-15 extends to lower Al₂O₃ and Na₂O
777 and to higher K₂O and to higher HFSE concentrations (Fig.6d). Therefore, we
778 cannot confirm a correlation between VRa and TM-15. Furthermore, TM-15 lacks
779 a phono-trachytic component, but this may be an artefact of sampling from the
780 base of the visible tephra layer.

781

782 TM-15 has been linked to the distal Y-3 tephra, first described from an Ionian Sea
783 core (Keller 1978). The average major element data of Y-3 from the type-site
784 (Keller et al., 1978) overlaps with the TM-15 field defined in this study (Fig.7e,f).
785 Y-3 tephra has also been described from a number of locations in the
786 Mediterranean basin, including the Balkans (Wagner et al., 2008; Caron et al.,
787 2010) and in the Adriatic (Zanchetta et al., 2008; Calanchi et al., 1998; Bourne et
788 al., 2010), Ionian (Kraml, 1997) and Tyrrhenian (Munno and Petrosino, 2004;
789 Paterne et al., 1988) Seas. Of these studies, only the Tyrrhenian Sea data fall
790 within the compositional field of TM-15, while the Adriatic Sea data of Bourne et
791 al., (2010) lie on the same high-FeO and MgO trends but do not overlap with the
792 type site Y-3 type site of Keller (1978). It is possible that further correlations are
793 masked by averaged datasets, however some layers previously linked to Y-3
794 and/or TM-15 may be related to one or more of the other Pre-NYT eruptions.

795

796 *6.1.4 Campanian Ignimbrite (CI) & Y5/TM-18*

797

798 The phono-trachytic CI is clearly distinct from the trachytic Pre-CI magmas and
799 has lower CaO and K₂O and higher Na₂O relative to the younger NYT-series
800 magmas.

801

802 The CI is correlated with tephra layer TM-18 in Lago Grande di Monticchio
803 (Narcisi, 1996; Wulf et al., 2004). The TM-18 layer comprises a 17 cm thick basal
804 pumice fall layer overlain by a 9 cm thick layer of vitric ash, interpreted as the co-
805 ignimbrite fall deposit generated during the flow phase of the CI eruption by
806 Narcisi (1996) and Wulf et al. (2004). We have analysed the major and trace
807 element composition glasses from of both the basal pumice and the vitric ash
808 components of layer TM-18, here termed TM-18 base and TM-18 top,
809 respectively (Table 4). Compositions of TM-18 base glasses match that of
810 samples from the CI fall (Fig. 6, 7f), while TM-18 top glasses overlap completely
811 with the tephra sampled from the proximal CI lower and intermediate flows (Fig.
812 6, 7e).

813

814 The CI is correlated with the Y-5 ash layer, which is recognised from marine
815 cores across the Eastern Mediterranean (e.g. Cornell et al., 1983; Keller et al.,
816 1978) and the C-13 layer in the Tyrrhenian Sea (Paterne et al., 1988, Ton-That et
817 al., 2001). The CI is found in terrestrial sites as far as Russia, ~2500 km from the
818 source (Pyle et al., 2006; Giaccio et al, 2008). Costa et al. (2012) have modelled
819 the CI dispersal and show that >3.7 million km² was covered by >5 mm of ash.
820 The Y-5 tephra is significant from both a climatic viewpoint as it occurs near the

821 start of Heinrich event 4 (Ton-That et al., 2001) and an archaeological
822 perspective as it occurs within the timeframe of the European Middle to Upper
823 Palaeolithic transition (~40 ka BP, Fedele et al., 2008). Recorded occurrences of
824 the Y-5 tephra have a bimodal size distribution in some sites up to 1500 km from
825 the source (Cornell et al., 1983; Sparks and Huang, 1980), which may
826 correspond to both the fall and dilute pyroclastic current phases of the CI
827 eruption. The computational model of Costa et al. (2012) indicates that most of
828 the tephra dispersal was associated with the dilute pyroclastic density current
829 phase of the CI eruption.

830
831 Published bulk trace element compositions of distal CI tephra fall from the
832 Aegean (Hardiman et al., 1999; Pyle et al., 2006) and Tyrrhenian (Paterne 1988;
833 Ton-That et al., 2001) seas and from continental settings in Lesvos, Greece
834 (Margari et al., 2007), Dobrogea, Romania (Veres et al., 2012), lakes Ohrid and
835 Prespa, Macedonia (Sulpizio et al., 2010); Crvena Stijena, Montenegro (Morley
836 and Woodward 2011) and Kostenki-Borschevo, Russia (Pyle et al., 2006) lie
837 close to the boundary between CI fall and CI lower and intermediate flow on plots
838 of Zr-Th. Therefore it is not possible to determine whether the fall or flow phase is
839 dominant in these locations. However, these discriminators provide the possibility
840 of further detailing the dispersal of the two main phases of the CI eruption, as full
841 trace element glass datasets become available for distal occurrences of CI
842 tephra.

843
844 The upper flow, represented by the samples from San Marco Evangelista quarry
845 (this work and Arienzo et al., 2009), is considered to have been produced by the
846 last and least energetic eruptive phase of low volume (~20 km³) and high
847 viscosity magma (Civetta et al., 1997). Proximally, the CI upper flow is restricted
848 mainly to the Campanian Plain, but may have fuelled detached, dilute co-
849 ignimbrite clouds that carried ash distally. A single TM-18 top shard from the
850 distal Lago Grande di Monticchio corresponds to the composition of the CI upper
851 flow. More distally, Sulpizio et al., (2010) report the occurrence of three differently
852 evolved trachytic magmas in Lakes Ohrid and Prespa (Macedonia), one of which
853 corresponds to the upper flow. However, the upper flow is not widely reported in
854 distal settings. We use the ratio of Na₂O/K₂O <0.6 to distinguish the CI Upper
855 Flow in published datasets of distal CI tephra, in cases where compositional data
856 is given for individual glass shards. CI upper flow tephra is present at Kostenki-
857 Borschevo, Russia (Pyle et al., 2006), Dobrogea, Romania (Veres et al., 2012),
858 Crvena Stijena, Montenegro (Morley and Woodward 2011), Lakes Ohrid and
859 Prespa, Macedonia (Sulpizio et al., 2010, Caron et al., 2010, Wagner et al., 2008,
860 Vogel et al., 2010), Lesvos, Greece (Margari et al., 2007) and Philippi, Greece
861 (St.Seymour et al., 2004). In most cases, the CI upper flow only constitutes a
862 minor proportion of the population of CI tephra shards and its presence in other
863 localities may be masked in averaged datasets. Our analysis of published
864 datasets suggests that the CI upper flow is widely present.

865
866 *6.1.5 Pre-Campanian Ignimbrite*

867

868 The Pre-CI units described here (TLa, TLc and TLf from Trefola) all have
869 restricted compositional ranges and can be distinguished from the CI on the
870 basis of major element composition.

871

872 Many of the Pre-CI tephra are likely to be widely dispersed across the
873 Mediterranean because of their proximal thicknesses and eastward dispersal (Di
874 Vito et al., 2008). West of the Apennines, TLc in the Trefola Quarry has been
875 linked to the Santa Lucia fall deposits with an age 50.95 ± 2.98 cal ka BP on the
876 basis of glass major and whole rock trace element data (Di Vito et al., 2008). The
877 Santa Lucia deposits are widespread and thick in the Apennine area and are also
878 reported in the Camaldoli della Torre core (Santa Lucia) from the southern slopes
879 of Somma-Vesuvius (Di Renzo et al., 2007). However, the EDS glass data for
880 Santa Lucia (Di Vito et al., 2008) differs significantly from the TLc data presented
881 here, having higher CaO, K₂O and MgO and lower Na₂O. The trace element
882 composition of Santa Lucia pumices has lower levels of trace element
883 enrichment relative to TLc.

884

885 **6.2 Implications for tephra correlations**

886

887 This study of proximal glass major and trace element geochemistries from the
888 60-12 ka eruptive sequence of the Phlegraean Fields highlights several issues of
889 relevance for tephrochronology.

890

891 *6.2.1 Exposure*

892

893 Incomplete preservation due to erosion and limited exposure in urban areas at
894 proximal localities means that some tephra units preserved distally may not be
895 recognised proximally. For example, we are unable to identify a proximal
896 equivalent of the distal Lago Grande di Monticchio TM-18-4 and TM-15 tephra
897 layers. For this reason, there is a need for high quality major and trace element
898 glass datasets from high-resolution distal archives such as the Lago Grande di
899 Monticchio, and from other type sites in medial-distal locations.

900

901 *6.2.2 Stratigraphic variation*

902

903 Proximal deposits from the large CI and NYT eruptions show compositional
904 variation with stratigraphic height, reflecting heterogeneous magma systems. The
905 range of geochemistries is an additional feature which can be used to
906 characterise a given eruption for the purpose of correlating tephras. For example
907 we are able to distinguish the Plinian fall and dilute pyroclastic flow phases of the
908 CI, and the lower and Upper Members of the NYT. For this reason, average
909 tephra compositions should not be presented; representative analyses are more
910 informative and whole datasets are desirable. It is critical that samples are taken
911 vertically through distal tephra layers to ensure they are representative.

912

913 6.2.3 *Long lived magma systems*

914

915 Both the 60-39 ka (CI-series) and 39-14 ka (NYT-series) time windows are
916 characterised by magma systems which erupted several times and produced
917 tephra which either overlap extensively or are indistinguishable in composition.
918 This is also observed for the more recent eruptions from the Phlegraean Fields
919 (Smith et al., 2011). Therefore, it is important to consider other close-in-time and
920 geochemically similar magmas from a potential source volcano when assigning
921 proximal-distal and distal-distal tephra correlations. At the Phlegraean Fields, the
922 proximal Pre-NYT units VRa, VRb and PRa cannot be clearly distinguished using
923 major and trace element glass geochemistry. The same holds true for the Pre-CI
924 TLa and TLc. In the absence of a definitive geochemical fingerprint, good
925 stratigraphic, chronological, sedimentological control is required and additional
926 characteristics of the deposit, such as clast shape, external surface, groundmass
927 texture are also important (e.g. Cioni et al., 2008).

928

929 6.2.4 *Petrogenesis*

930

931 The consistency of U, Th, Nb, Ta, Zr, and Y inter-element ratios (Fig. 5) within
932 the CI-series glasses indicates that they share a parental magma, in agreement
933 with the findings of Arienzo et al. (2009), D'Antonio et al. (2007), Di Renzo et al.
934 (2011) and Pabst et al. (2008). Differences between the CI-series magmas
935 primarily reflect differing degrees of differentiation, but there is no systematic
936 increase in the degree of differentiation with time, suggesting that the CI-series
937 magmas do not reflect a single evolving magma chamber, but instead reflect
938 distinct magma batches which originated from the parental magma at depth and
939 fractionated in separate shallow reservoirs, as shown by Pabst et al. (2008). This
940 excludes the last erupted magma, the CI upper flow, which is distinct from other
941 magmas in the CI-series. Its composition is less differentiated than the CI fall and
942 the lower and intermediate flows and defines a mixing trend between the CI fall
943 and a less differentiated magma.

944

945 The NYT-series and the PP glasses have consistent HFSE/Th ratios and likely
946 share a similar parent. The NYT-series and PP magmas form compositional
947 clusters and do not define a single differentiation trend. However, these younger
948 magmas have lower U, Th, Nb, Ta, Zr, and Y concentrations and lower HFSE/ Th
949 ratios (Fig. 5) relative to the CI-series, indicating that the NYT-series/PP magmas
950 originated from a different parental magma to the older series. These results
951 agree with previous work suggesting isotopically and geochemically different
952 magmas for the CI-series and the NYT-series/PP (Arienzo et al., 2009; Di Renzo
953 et al., 2007; Di Renzo et al., 2011; Pabst et al., 2008; Pappalardo et al., 1999;
954 Pappalardo et al., 2002a; Pappalardo et al., 2002b; D'Antonio et al., 2007;
955 Tonarini et al., 2004). Understanding the petrogenetic processes operating at the
956 Phlegraean Fields means that we can assign an unknown Phlegraean Fields
957 tephra to the appropriate series, even in the absence of a proximal match,

958 because the HFSE/Th ratio is indicative of a certain parental magma (CI-series
959 magma and NYT-series/PP magma).

960
961 Where multiple eruptions produce identical tephra, such as the Pre-NYT, it may
962 be possible to define compositional groups. Pabst et al. (2008) identified three
963 distinct Pre-CI magma batches that were erupted sequentially. Bracketing the
964 age of the first and last occurrence of each compositional group may be useful in
965 providing age constraints on an unknown Phlegraean Fields distal tephra. This
966 could be achieved either by dating of proximal samples or using high-resolution
967 distal archives, such as Lago Grande di Monticchio.

968 **7. CONCLUSIONS**

969
970
971 The 60-12 ka eruptive sequence of Phlegraean Fields offers an ideal case study
972 to investigate proximal-distal tephra correlations because of the large number of
973 eruptions recorded proximally and in the medial-distal Lago Grande di Monticchio
974 core. The micron-beam major and trace element glass dataset presented here
975 indicate that:

- 976
977 1. CI-series (60-39 ka) and NYT-series/PP magmas (39-12 ka) were derived
978 from geochemically different magmas, in agreement with previous isotopic
979 studies (Di Renzo et al. (2011), and references therein). HFSE/Th and
980 FeO/CaO ratios are constant within each series, allowing an unknown
981 Phlegraean Fields tephra to be assigned to the appropriate series, even if
982 the exact proximal equivalent is not known.
- 983 2. Tephra from the caldera forming NYT eruption compositionally overlaps
984 with tephra from the smaller Pre-NYT eruptions. The NYT may be
985 distinguished by the presence of the bimodal trachytic and phono-trachytic
986 LM and by the UM, which spans a compositional range between trachyte
987 and phonotrachyte. Assessment of published data for distal occurrences
988 of NYT tephra shows that the UM is the dominant NYT tephra in settings
989 to the east and west of Phlegraean Fields. However, the NYT-LM is found
990 in the absence of the NYT-UM in locations to the far north of Phlegraean
991 Fields.
- 992 3. Magma erupted during the caldera forming CI event straddle the phono-
993 trachyte and is distinct from the preceding, lower volume Pre-CI magmas
994 in major and trace element composition. CI glasses from the Plinian (fall)
995 and the lower and intermediate flow phases of the eruption overlap
996 extensively, but can be separated using a plot of Zr-Th.
- 997 4. There is extensive overlap in major and trace element composition within
998 Pre-NYT and within the Pre-CI, making it extremely difficult to assign
999 proximal-distal and distal-distal correlations. This means that some such
1000 correlations may not be correct. For example, we show that the TM-15
1001 layer from Lago Grande di Monticchio is not the distal equivalent of VRa. It
1002 may be possible to recognize the compositional group of an unknown

1003 distal Phlegraean Fields tephra and therefore constrain its stratigraphic
1004 position and age.

1005
1006 In addition to insights into the behavior of the magmatic feeding system,
1007 proximal-distal tephra correlations of single eruptions are important for the
1008 assessment of volcanic hazards, for example zoning of territory in relation to
1009 various dangerous eruption phenomena. Proximal-distal tephra correlations allow
1010 more precise estimates of the volume of magma extruded during a single
1011 eruption and, therefore, the definition of the eruption magnitude and intensity.
1012 Knowledge of such parameters for past eruptions of an active volcano is
1013 fundamental to evaluation of the effects of such an eruption on the environment
1014 and on climate. This is particularly relevant for volcanoes located in densely
1015 populated areas, such as the Phlegraean Fields caldera located in the densely
1016 inhabited Neapolitan area of southern Italy. The results of this study will
1017 contribute to the ongoing improvement of current volcanic hazards assessments
1018 (Orsi et al., 2004; 2009; Costa et al., 2009; Selva et al., 2012).

1019
1020 *Acknowledgements: This work is funded by the NERC RESET Consortium*
1021 *(NE/E015905/1). This is paper number ROX/0020. The authors wish to thank*
1022 *Roberto Sulpizio and two anonymous reviewers for thorough and constructive*
1023 *feedback; Paul Albert and Chris Satow for useful discussions and Neil Holloway*
1024 *for sample preparation.*

1025 1026 **REFERENCES**

- 1027
1028 Arienzo I., Civetta L., Heumann A., Wörner G., and Orsi G. (2009) Isotopic
1029 evidence for open system processes within the Campanian Ignimbrite
1030 (Campi Flegrei, Italy) magma chamber. *B. Volcanol.* **71**(3), 285-300.
1031 Andronico, D., Calderoni, G., Cioni, R., Donahue, D.J., Marianelli, P., Santacroce,
1032 R., Sbrana, A., Sulpizio, R. (1996) An Updated Chronostratigraphic Scheme
1033 of the Last 19,000 Years of Vesuvius Magmatic and Eruptive History. EOS,
1034 Electronic Supplement to the Member Newspaper of the American
1035 Geophysical Union (AGU), November 7 1996, 671-672.
1036 Arienzo I., Heumann A., Wörner G., Civetta L., and Orsi G. (2011) Processes and
1037 timescales of magma evolution prior to the Campanian Ignimbrite eruption
1038 (Campi Flegrei, Italy). *Earth Planet. Sci. Lett.* **306**(3-4), 217-228.
1039 Arienzo I., Moretti R., Civetta L., Orsi G., and Papale P. (2010) The feeding
1040 system of Agnano Monte Spina eruption (Campi Flegrei, Italy): Dragging the
1041 past into present activity and future scenarios. *Chem. Geol.* **270**(1-4), 135-
1042 147.
1043 Aufebauer, A., Panagiotopoulos, K., Wagner, B., Schaebitz, F., Viehberg, F.A.,
1044 Vogel, H., Zanchetta, G., Sulpizio, R., Leng, M.J. and Damaschke, M. (in
1045 press) Climate and environmental change in the Balkans over the last 17 ka
1046 recorded in sediments from Lake Prespa (Albania/F.Y.R. of
1047 Macedonia/Greece). *Quatern. Int.*

- 1048 Barberi F., Innocenti F., Lirer L., Munno R., Pescatore T., and Santacroce R.
 1049 (1978) The campanian ignimbrite: a major prehistoric eruption in the
 1050 Neapolitan area (Italy). *B. Volcanol.*, Vol. 41, 10-31.
- 1051 Bohrson W. A., Spera F. J., Fowler S. J., Belkin H. E., De Vivo B., and Rolandi G.
 1052 (2006) *Chapter 13 Petrogenesis of the Campanian Ignimbrite: implications*
 1053 *for crystal-melt separation and open-system processes from major and*
 1054 *trace elements and Th isotopic data.* In *Developments in Volcanology*, 9(C),
 1055 249-288.
- 1056 Bourne A. J., Lowe J. J., Trincardi F., Asioli A., Blockley S. P. E., Wulf S.,
 1057 Matthews I. P., Piva A., and Vigliotti L. (2010) Distal tephra record for the
 1058 last ca 105,000 years from core PRAD 1-2 in the central Adriatic Sea:
 1059 implications for marine tephrostratigraphy. *Quaternary Sci. Rev.*, **29**(23-24),
 1060 3079-3094.
- 1061 Bourne, A.J., (2012) The late Quaternary tephrochronology of the Adriatic Region:
 1062 implications for the synchronisation of marine records. University of London,
 1063 unpublished PhD Thesis
- 1064 Brandt U., Nowaczyk N. R., Ramrath A., Brauer A., Mingram J., Wulf S., and
 1065 Negendank J. F. W. (1999) Palaeomagnetism of Holocene and Late
 1066 Pleistocene sediments from Lago di Mezzano and Lago Grande di
 1067 Monticchio (Italy): initial results. *Quaternary Sci Rev* **18**, 961-976.
- 1068 Brauer A., Mingram J., Frank U., Gunter C., Schettler G., Wulf S., Zolitschka B.,
 1069 and Negendank J. F. W. (2000) Abrupt environmental oscillations during the
 1070 Early Weichselian recorded at Lago Grande di Monticchio, southern Italy.
 1071 *Quatern. Int.* **73/74**, 79-90.
- 1072 Calanchi N., Cattaneo A., Dinelli E., Gasparotto G., and Lucchini F. (1998) Tephra
 1073 layers in Late Quaternary sediments of the central Adriatic Sea. *Mar. Geol.*,
 1074 **149**(1-4), 191-209.
- 1075 Calanchi, N, Dinelli, E. (2008) Tephrostratigraphy of the last 170 ka in sedimentary
 1076 successions from the Adriatic Sea. *J. Volcan. Geoth. Res.*, **177** (1), 81-95.
- 1077 Caron, B., Sulpizio, R., Zanchetta, G., Siani, G. and Santacroce, R. (2010) The
 1078 Late Holocene to Pleistocene tephrostratigraphic record of Lake Ohrid
 1079 (Albania). *C. R. Geosci.*, **342** (96), 453-466.
- 1080 Cioni R., D'Oriano, C., Bertagnini A. (2008). Fingerprinting ash deposits of small
 1081 scale eruptions by their physical and textural features. *J. Volcan. Geoth.*
 1082 *Res.* **177**, 277-287
- 1083 Civetta L., Orsi G., Pappalardo L., Fisher R. V., Heiken G., and Ort M. (1997)
 1084 Geochemical zoning, mingling, eruptive dynamics and depositional
 1085 processes - The Campanian Ignimbrite, Campi Flegrei caldera, Italy. *J.*
 1086 *Volcan. Geoth. Res.*, **75**(3-4), 183-219.
- 1087 Cornell W., S. Carey S., and Sigurdsson H. (1983) Computer simulation of
 1088 transport and deposition of Campanian Y-5 ash. *J. Volcan. Geoth. Res.*, **17**,
 1089 89-109.
- 1090 Costa A., Dell'Erba F., Di Vito M., Isaia R., Macedonio G., Orsi G., Pfeiffer T.
 1091 (2009) Tephra fallout hazard assessment at the Campi Flegrei caldera
 1092 (Italy) *B. Volcan.*, **71**, 259-273
- 1093 Costa, A., Folch, A., Macedonio, G., Giaccio, B., Isaia, R., Smith, V.C. (2012)

1094 Quantifying volcanic ash dispersal and impact of the Campanian Ignimbrite
1095 super-eruption, *Geophys. Res. Lett.*, 39 doi:10.1029/2012GL051605.

1096 D'Antonio M., Tonarini S., Arienzo I., Civetta L., and Di Renzo V. (2007)
1097 Components and processes in the magma genesis of the Phlegraean
1098 Volcanic District, Southern Italy. In *Cenozoic volcanism in the*
1099 *Mediterranean area*, Vol. 418 (ed. L. Beccaluva, G. Bianchini, and M.
1100 wilson), pp. 203-220. Geological Society of America Special Publication.

1101 De Vivo B., Rolandi G., Gans P. B., Calvert A., Bohrson W. A., Spera F. J., and
1102 Belkin H. E. (2001) New constraints on the pyroclastic eruptive history of
1103 the Campanian volcanic Plain (Italy). *Miner. Petrol.*, **73**(1-3), 47-65.

1104 Deino A. L., Orsi G., de Vita S., and Piochi M. (2004) The age of the Neapolitan
1105 Yellow Tuff caldera-forming eruption (Campi Flegrei caldera Italy) assessed
1106 by Ar-40/Ar-39 dating method. *J. Volcan. Geoth. Res.*, **133**(1-4), 157-170.

1107 Di Renzo V., Arienzo I., Civetta L., D'Antonio M., Tonarini S., Di Vito M. A., and
1108 Orsi G. (2011) The magmatic feeding system of the Campi Flegrei caldera:
1109 Architecture and temporal evolution. *Chem. Geol.* **281**(3-4), 227-241.

1110 Di Renzo V., Di Vito M. A., Arienzo I., Carandente A., Civetta L., D'Antonio M.,
1111 Giordano F., Orsi G., and Tonarini S. (2007) Magmatic history of Somma-
1112 Vesuvius on the basis of new geochemical and isotopic data from a deep
1113 borehole (Camaldoli della Torre). *J. Petrol.*, **48**(4), 753-784.

1114 Di Vito M. A., Isaia R., Orsi G., Southon J., de Vita S., D'Antonio M., Pappalardo
1115 L., and Piochi M. (1999) Volcanism and deformation since 12,000 years at
1116 the Campi Flegrei caldera (Italy). *J. Volcan. Geoth. Res.*, **91**(2-4), 221-246.

1117 Di Vito M. A., Sulpizio R., Zanchetta G., and D'Orazio M. (2008) The late
1118 Pleistocene pyroclastic deposits of the Campanian Plain: new insights into
1119 the The late Pleistocene pyroclastic deposits of the Campanian Plain: new
1120 insights into the explosive activity of Neapolitan volcanoes. *J. Volcan.*
1121 *Geoth. Res.*, 177(1), 19-48.

1122 De Vivo B., Rolandi G., Gans P.B., Calvert A., Bohrson W.A., Spera F.J. and
1123 Belkin H.E. (2001) New constraints on the pyroclastic eruptive history of the
1124 Campanian volcanic Plain (Italy). In: De Vivo B, Rolandi G (eds) Mt Somma
1125 Vesuvius and Volcanism of the Campania Plain. Spec Issue Mineral Petrol
1126 73:47–65.

1127 D'Oriano C., Poggianti E., Bertagnini A., Cioni R., Landi P., Polacci M., and Rosi
1128 M. (2005) Changes in eruptive style during the A.D. 1538 Monte Nuovo
1129 eruption (Phlegrean Fields, Italy): the role of syn-eruptive crystallisation. *B.*
1130 *Volcan.*, **67**, 601-621.

1131 Fedele F. G., Giaccio B., Isaia R., and Orsi G. (2003) The Campanian Ignimbrite
1132 eruption, Heinrich Event 4, and Palaeolithic change in Europe: a high-
1133 resolution investigation. *AGU Geophys. Monogr.* **139**, 301-327.

1134 Fedele F. G., Giaccio B., Isaia R., Orsi G., Carroll M., and Scaillet B. (2007) The
1135 Campanian Ignimbrite Factor: Towards a Reappraisal of the Middle to
1136 Upper Palaeolithic "Transition". In *Living Under the Shadow: The Cultural*
1137 *Impacts of Volcanic Eruptions* (ed. J. G. a. R.Torrence), pp. 19-41. Left
1138 Coast Press.

- 1139 Fedele L., Scarpati C., Lanphere M., Melluso L., Morra V., Perrotta A., and Ricci
 1140 G. (2008) The Breccia Museo formation, Campi Flegrei, southern Italy:
 1141 geochronology, chemostratigraphy and relationship with the Campanian
 1142 Ignimbrite eruption. *B. Volcan.*, **70**(10), 189-1219.
- 1143 Fisher R. V., Orsi G., Ort M., and Heiken G. (1993) Mobility of a Large-Volume
 1144 Pyroclastic Flow - Emplacement of the Campanian Ignimbrite, Italy. *177*(1),
 1145 19-48 **56**(3), 205-220.
- 1146 Fowler S. J., Spera F., Bohrson W., Belkin H. E., and De Vivo B. (2007) Phase
 1147 equilibria constraints on the chemical and physical evolution of the
 1148 campanian ignimbrite. *J. Petrol.* **48**(3), 459-493.
- 1149 Giaccio, B., Isaia, R., Fedele, F. G., Di Canzio, E., Hoffecker, J., Ronchitelli, A.,
 1150 Sinitsyn, A., Anikovich, M., and Lisitsyn, S. N. (2008). The Campanian
 1151 Ignimbrite and Codola tephra layers: two temporal/stratigraphic markers for
 1152 the Early Upper Palaeolithic in southern Italy and eastern Europe, *J.*
 1153 *Volcan. Geoth. Res.*, **177**, 208–226.
- 1154 Hardiman J. C. (1999) Deep sea tephra from Nisyros Island, eastern Aegean Sea,
 1155 Greece. In *Volcanoes in the Quaternary*, Vol. **161** (ed. C. R. Firth and W. J.
 1156 McGuire), 69-88. Geological Society, London, Special Publications.
- 1157 Jarosewich, E., 2002. Smithsonian Microbeam Standards. *Journal of Research of*
 1158 *the National Institute of Standards and Technology*, *107*(6): 681–685.
- 1159 Jochum, K.P. et al., 2006. MPI-DING reference glasses for in situ microanalysis:
 1160 New reference values for element concentrations and isotope ratios.
 1161 *Geochem. Geophys. Geosy.*, *7*(2).
- 1162 Keller J., Ryan W. B. F., Ninkovich D., and Altherr R. (1978) Explosive volcanic
 1163 activity in the Mediterranean over the past 200,000 yr as recorded in deep-
 1164 sea sediments. *Geol. Soc. Am. Bull.* **89**(4), 591-604.
- 1165 Kraml M. (1997) Laser-40Ar/39Ar-Datierungen an distalen marinen Tephren des
 1166 jung-quart.aren mediterranen Vulkanismus. Ph.D, Albert-Ludwigs-Universit.
- 1167 Lane C. S., Andric M., Cullen V. L., and Blockley S. P. E. (2011) The occurrence
 1168 of distal Icelandic and Italian tephra in the Lateglacial of Lake Bled,
 1169 Slovenia. *Quaternary Sci. Rev.*, **30**(9-10), 1013-1018.
- 1170 Le Bas M. J. and Streckeisen A. L. (1991) The IUGS systematics of igneous rocks.
 1171 *Journal of the Geological Society* **148**(5), 825-833.
- 1172 Lirer L., Petrosino P., and Alberico I. (2001) Hazard assessment at volcanic fields:
 1173 the Campi Flegrei case history. *J. Volcan. Geoth. Res.*, **112**(1-4), 53-73.
- 1174 Magny, M., de Beaulieu, J.-L., Drescher-Schneider, R., Vanni ere, B., Walter-
 1175 Simonnet, A.-V., Millet, L., Bossuet, G. and Peyron, O. 2006. Climatic
 1176 oscillations in central Italy during the Last Glacial-Holocene transition: the
 1177 record from Lake Accesa. *J. Quaternary Sci.*, **21**, 311-320.
- 1178 Mangiacapra A., Moretti R., Rutherford M., Civetta L., Orsi G., and Papale P.
 1179 (2008) The deep magmatic system of the Campi Flegrei caldera (Italy).
 1180 *Geophys. Res. Lett.*, **35**, L21304.
- 1181 Margari V., Pyle D. M., Bryant C., and Gibbard P. L. (2007) Mediterranean tephra
 1182 stratigraphy revisited: Results from a long terrestrial sequence on Lesbos
 1183 Island, Greece. *J. Volcan. Geoth. Res.*, **163**(1-4), 34-54.

- 1184 Morley, M.W. and Woodward, J.C. (in press) The Campanian Ignimbrite (Y5)
1185 tephra at CrvenaStijena Rockshelter, Montenegro. *Quaternary Research*.
1186 Müller W., Shelley M., Miller P., and Broude S. (2009) Initial performance metrics
1187 of a new custom-designed ArF excimer LA-ICPMS system coupled to a
1188 two-volume laser-ablation cell. *J. Anal. Atom. Spectrom.*, **24**(2), 209-214.
1189 Munno R. and Petrosino P. (2004) New constraints on the occurrence of the Y-3
1190 upper Pliocene tephra marker layer in the Tyrrhenian Sea. *Il Quaternario*
1191 **17**(1), 11-20.
1192 Narcisi B. (1996) Tephrochronology of a late quaternary lacustrine record from the
1193 Monticchio maar (Vulture volcano, Southern Italy). *Quaternary Sci. Rev.*,
1194 **15**(2-3), 155-165.
1195 Orsi G., Civetta L., D'Antonio M., Di Girolamo P., and Piochi M. (1995) Step-
1196 Filling and Development of a 3-Layer Magma Chamber - the Neapolitan-
1197 Yellow-Tuff Case-History. *J. Volcan. Geoth. Res.*, **67**(4), 291-312.
1198 Orsi G., Civetta L., Del Gaudio C., de Vita S., Di Vito M. A., Isaia R., Petrazzuoli
1199 S., Ricciardi G., and Ricco C. (1999a) Short-Term Ground Deformations
1200 and Seismicity in the Nested Campi Flegrei Caldera (Italy): an example of
1201 active block resurgence in a densely populated area. *J. Volcan. Geoth.*
1202 *Res.*, **91**, 415-451.
1203 Orsi G., D'Antonio M., de Vita S., and Gallo G. (1992) The Neapolitan Yellow Tuff,
1204 a Large-Magnitude Trachytic PhreatoPlinian Eruption - Eruptive Dynamics,
1205 Magma Withdrawal and Caldera Collapse. *J. Volcan. Geoth. Res.*, **53**(1-4),
1206 275-287.
1207 Orsi G., de Vita S., Di Vito M. A., Isaia R., Nave R., and Heiken G. (2003) Facing
1208 volcanic and related hazards in the Neapolitan area. In *Earth Sciences in*
1209 *the Cities: A Reader*, Vol. 56 (ed. Heiken G., Fakundiny R., and Sutter J.),
1210 pp. 121-170. Am. Geophys. Un., Sp. Publ. Series.
1211 Orsi G., de Vita S., and Di Vito M. A. (1996) The restless, resurgent Campi Flegrei
1212 nested caldera (Italy): Constraints on its evolution and configuration. *J.*
1213 *Volcan. Geoth. Res.*, **74**(3-4), 179-214.
1214 Orsi G., Di Vito M. A., and Isaia R. (2004) Volcanic hazard assessment at the
1215 restless Campi Flegrei caldera. *B. Volcanol.*, **66**(6), 514-530.
1216 Orsi G., Petrazzuoli S., and Wohletz K. (1999b) Mechanical and thermo-fluid
1217 behaviour during unrest episode at the Campi Flegrei caldera (Italy). *J.*
1218 *Volcan. Geoth. Res.*, **91**, 453-470.
1219 Orsi G., Di Vito M.A., Selva J. and Marzocchi W. (2009) Long term forecast of
1220 eruption style and size at Campi Flegrei caldera (Italy). *E Planet Sci Let*
1221 **287**, 265-276
1222 Ort M., Orsi G., Pappalardo L., and Fisher R. (2003) Anisotropy of magnetic
1223 susceptibility studies of depositional processes in the Campanian
1224 Ignimbrite, Italy. *B. Volcanol.*, **65**(1), 55-72.
1225 Pabst S., Worner G., Civetta L., and Tesoro R. (2008) Magma chamber evolution
1226 prior to the Campanian Ignimbrite and Neapolitan Yellow Tuff eruptions
1227 (Campi Flegrei, Italy). *B. Volcanol.*, **70**(8), 961-976.
1228 Pappalardo L., Civetta L., D'Antonio M., Deino A., Di Vito M.A., Orsi G.,
1229 Carandente A., de Vita S., Isaia R., and Piochi M. (1999) Chemical and Sr-

- 1230 isotopical evolution of the Phlegraean magmatic system before the
 1231 Campanian Ignimbrite and the Neapolitan Yellow Tuff eruptions. *J. Volcan.
 1232 Geoth. Res.*, **91**(2-4), 141-166.
- 1233 Pappalardo L., Civetta L., de Vita S., Di Vito M. A., Orsi G., Carandente A., and
 1234 Fisher R. V. (2002a) Timing of magma extraction during the Campanian
 1235 Ignimbrite eruption (Campi Flegrei Caldera). *J. Volcan. Geoth. Res.*, **114**(3-
 1236 4), 479-497.
- 1237 Pappalardo L., Ottolini L., and Mastrolorenzo G. (2008) The Campanian Ignimbrite
 1238 (southern Italy) geochemical zoning: insight on the generation of a super-
 1239 eruption from catastrophic differentiation and fast withdrawal. *Contrib.
 1240 Mineral. and Petr.*, **156**(1), 1-26.
- 1241 Pappalardo L., Piochi M., D'Antonio M., Civetta L., and Petrini R. (2002b)
 1242 Evidence for multi-stage magmatic evolution during the past 60 kyr at
 1243 Campi Flegrei (Italy) deduced from Sr, Nd and Pb isotope data. *J. Petrol.*,
 1244 **43**(8), 1415-1434.
- 1245 Paterne M., Guichard F., and Labeyrie J. (1988) Explosive activity of the South
 1246 Italian volcanoes during the past 80,000 years as determined by marine
 1247 tephrochronology. *J. Volcan. Geoth. Res.*, **34**(3-4), 153-172.
- 1248 Paterne M., Guichard F., and Labeyrie J. (1988) Explosive activity of the South
 1249 Italian volcanoes during the past 80,000 years as determined by marine
 1250 tephrochronology. *J. Volcan. Geoth. Res.*, **34**(3-4), 153-172.
- 1251 Perrotta A. and Scarpati C. (2003) Volume partition between the Plinian and co-
 1252 ignimbrite air fall deposits of the Campanian Ignimbrite eruption. *Miner
 1253 Petrol.*, **79**, 67-78.
- 1254 Polacci M., Pioli L., and Rosi M. (2003) The Plinian phase of the Campanian
 1255 Ignimbrite eruption (Phlegrean Fields, Italy): evidence from density
 1256 measurements and textural characterization of pumice. *B. Volcanol.*, **65**(6),
 1257 418-432.
- 1258 Pyle D. M., Ricketts G. D., Margari V., van Andel T. H., Sinitsyn A. A., Praslov N.
 1259 D., and Lisitsyn S. (2006) Wide dispersal and deposition of distal tephra
 1260 during the Pleistocene 'Campanian Ignimbrite/Y5' eruption, Italy.
 1261 *Quaternary Sci. Rev.*, **25**(21-22), 2713-2728.
- 1262 Reimer P. J., Baillie M. G. L., Bard E., Bayliss A., Beck J. W., Blackwell P. G.,
 1263 Bronk Ramsey C., Buck C. E., Burr G. S., Edwards R. L., Friedrich M.,
 1264 Grootes P. M., Guiderson T. P., Hajdas I., Heaton T. J., Hogg A. G.,
 1265 Hughen K. A., Kaiser K. F., Kromer B., McCormac F. G., Manning S. W.,
 1266 Richards D. A., Southon J. R., Talamo S., Turney C. S. M., van der Plicht
 1267 J., and Weyhenmeyer C. E. (2009) IntCal09 and Marine09 radiocarbon age
 1268 calibration curves, 0-50,000 years cal BP. *Radiocarbon* **51**(4), 1111-1150.
- 1269 Rittmann A. (1950) Sintesi geologica dei Campi Flegrei. *Boll. Soc. Geol. Ital.* **69**,
 1270 117-177.
- 1271 Rolandi G., Bellucci F., Heizler M. T., Belkin H. E., and De Vivo B. (2003) Tectonic
 1272 controls on the genesis of ignimbrites from the Campanian Volcanic Zone,
 1273 southern Italy. *Miner. Petrol.*, Vol. 79, pp. 3-31.

- 1274 Rosi M., Vezzoli L., Castelmenzano A., and Grieco G. (1999) Plinian pumice fall
 1275 deposit of the Campanian Ignimbrite eruption (Phlegraean Fields, Italy).
 1276 *Journal of Volcanology and Geothermal Research* **91**(2-4), 179-198.
- 1277 Santacroce R., Cristofolini R., La Volpe, L., Orsi G., and Rosi M. (2003) Italian
 1278 Active Volcanoes. *Episodes* **26**(3), 227-234.
- 1279 Schmidt R., van den Bogaard C., Merkt J., and Müller J. (2002) A new Lateglacial
 1280 chronostratigraphic tephra marker for the south-eastern Alps: The
 1281 Neapolitan Yellow Tuff (NYT) in Längsee (Austria) in the context of a
 1282 regional biostratigraphy and palaeoclimate. *Quatern. Int.*, **88**(1), 45-56.
- 1283 Selva J., Orsi G., Di Vito M.A., Marzocchi W. and Sandri L. (2012) Probability
 1284 hazard map for future vent opening at the Campi Flegrei caldera, Italy. *B.*
 1285 *Volcan.*, **74**, 497-510
- 1286 Seymour, St K., Christanis, K., Bouzinos, A., Papazisimou, S., Papatheodorou, G.,
 1287 Moran, E. and Denes, G., 2004. Tephrostratigraphy and tephrochronology
 1288 in the Philippi peat basin, Macedonia, Northern Hellas (Greece). *Quatern.*
 1289 *Int.*, **121**, 53-65.
- 1290 Siani G., Sulpizio R., Paterne M., and Sbrana A. (2004) Tephrostratigraphy study
 1291 for the last 18,000 C-14 years in a deep-sea sediment sequence for the
 1292 South Adriatic. *Quaternary Science Reviews* **23**(23-24), 2485-2500.
- 1293 Smith V. C., Isaia R., and Pearce N. J. (2011) Tephrostratigraphy and glass
 1294 compositions of post-15 kyr Campi Flegrei eruptions: implications for
 1295 eruption history and chronostratigraphic markers. *Quaternary Sci. Rev.*
 1296 **30**(25-26), 638–3660.
- 1297 Sparks R. S. J. and T.C. H. (1980) The volcanological significance of deep-sea
 1298 ash layers associated with ignimbrites. *Geol. Mag.* **117**, 425–436.
- 1299 Sulpizio R. (2005). Three empirical methods for the calculation of distal volume of
 1300 tephra-fall deposits. *J. Volcan. Geoth. Res.*, **145**(3-4), 315-336.
- 1301 Sulpizio R., Zanchetta G., D'Orazio M., Vogel H., Wagner B. (2010)
 1302 Tephrostratigraphy and tephrochronology of lakes Ohrid and Prespa,
 1303 Balkans. *Biogeosciences*, **7**, 3273-3288.
- 1304 Sulpizio R., van Welden A., Caron B., Zanchetta G. (2010) The Holocene
 1305 tephrostratigraphic record of Lake Shkodra (Albania and Montenegro). *J.*
 1306 *Quaternary Sci.*, **25**, 633-650.
- 1307 Sun S.-S. and McDonough W. F. (1989) Chemical and isotopic systematics of
 1308 oceanic basalts: implications for mantle composition and processes. In
 1309 *Magmatism in Ocean Basins*, Vol. 42 (ed. A. D. Saunders, Norry, M.J.), pp.
 1310 313-345. Geological Society of London Special Publication.
- 1311 Thirlwall M. F. (1991) Long-Term Reproducibility of Multicollector Sr and Nd
 1312 Isotope Ratio Analysis. *Chem. Geol.* **94**(2), 85-104.
- 1313 Thunell R., Federman A., Sparks S., and Williams D. (1979) The age, origin, and
 1314 volcanological significance of the Y-5 ash layer in the Mediterranean.
 1315 *Quaternary Research* **12**(2), 241-253.
- 1316 Tomlinson E. L., Thordarson T., Muller W., Thirlwall M., and Menzies M. A. (2010)
 1317 Micro analysis of tephra by LA-ICP-MS - strategies, advantages and
 1318 limitations assessed using the Thorsmork ignimbrite (Southern Iceland).
 1319 *Chem. Geol.* **279**(3-4), 73-89.

- 1320 Tonarini S., Leeman W. P., Civetta L., D'Antonio M., Ferrara G., and Necco A.
 1321 (2004) B/Nb and systematics in the Phlegrean Volcanic District (PVD). *J.*
 1322 *Volcan. Geoth. Res.*, **113**, 123-139.
- 1323 Ton-That T., Singer B., and Paterne M. (2001) $^{40}\text{Ar}/^{39}\text{Ar}$ dating of latest
 1324 Pleistocene (41 ka) marine tephra in the Mediterranean Sea: implications
 1325 for global climate records. *Earth Planet. Sci. Lett.*, **184**(3-4), 645-658.
- 1326 Veres, D., Lane, C.S., Timar-Gabor, A., Hambach, U., Constantin, D., Szakács, A.,
 1327 Fülling, A. and Onac, B.P. (in press). The Campanian Ignimbrite/Y5 tephra
 1328 layer - A regional stratigraphic marker for Isotope Stage 3 deposits in the
 1329 Lower Danube region. *Quatern. Int.*
- 1330 Vezzoli L. (1991) Tephra layers in Bannock Basin (Eastern Mediterranean). *Mar.*
 1331 *Geol.*, **100**(1-4), 21-34.
- 1332 Vogel H., Zanchetta G., Sulpizio R., Wagner B., Nowaczyk N. (2010). A
 1333 tephrostratigraphic record for the last glacial-interglacial cycle from Lake
 1334 Ohrid, Albania and Macedonia. *J. Quaternary Sci.*, **25**, 320-338.
- 1335 Wagner B., Sulpizio R., Zanchetta G., Wulf S., Wessels M., Daut G., and
 1336 Nowaczyk N. (2008) The last 40 ka tephrostratigraphic record of Lake
 1337 Ohrid, Albania and Macedonia: a very distal archive for ash dispersal from
 1338 Italian volcanoes. *J. Volcan. Geoth. Res.*, **177**(1), 71-80.
- 1339 Wohletz K., Civetta L., and Orsi G. (1999) Thermal evolution of the Phlegrean
 1340 magmatic system. *J. Volcan. Geoth. Res.*, **91**(2-4), 381-414.
- 1341 Wohletz K., Orsi G., and de Vita S. (1995) Eruptive Mechanisms of the Neapolitan
 1342 Yellow Tuff Interpreted from Stratigraphic, Chemical, and Granulometric
 1343 Data. *J. Volcan. Geoth. Res.*, **67**, 263-290.
- 1344 Wulf S., Brauer A., Mingram J., Zolitschka B., and Negendank J. F. W. (2007)
 1345 Distal tephras in the sediments of Monticchio maar lakes. In *Geologia del*
 1346 *Monte Vulture* (ed. C. Principe), pp. 105-122.
- 1347 Wulf S., Kraml M., Brauer A., Keller J., and Negendank J. F. W. (2004)
 1348 Tephrochronology of the 100 ka lacustrine sediment record of Lago Grande
 1349 di Monticchio (southern Italy). *Quatern. Int.*, **122**, 7-30.
- 1350 Wulf S., Kraml M., and Keller J. (2008) Towards a detailed distal
 1351 tephrostratigraphy in the Central Mediterranean: The last 20,000 yrs record
 1352 of Lago Grande di Monticchio. *J. Volcan. Geoth. Res.*, **177**(1), 118-132.
- 1353 Zanchetta G., Di Vito M.A., Fallick A. E., and Sulpizio R. (2000) Stable isotopes of
 1354 pedogenic carbonates from the Somma-Vesuvius area, Southern Italy, over
 1355 the past 18 kyr: paleoclimatic implications. *J. Quaternary Sci.*, **15**(8), 813-
 1356 824.
- 1357 Zanchetta G., Sulpizio R., Giaccio B., Siani G., Paterne M., Wulf S., and D'Orazio
 1358 M. (2008) The Y-3 tephra: A Last Glacial stratigraphic marker for the central
 1359 Mediterranean basin. *J. Volcan. Geoth. Res.*, **177**(1), 145-154.
- 1360 Zollo A., Maercklin N., Vassallo M., Dello Iacono D., Virieux J., and Gasparini P.
 1361 (2008) Seismic reflections reveal a massive melt layer under Campi Flegrei
 1362 volcanic field. *Geophys. Res. Lett.*, **244**(35), L12306.

1363
 1364
 1365

CAPTIONS

1366 **Tables**

1367

1368 Table 1: Summary of Phlegraean Fields eruptions and samples studied. Samples
1369 used in previous studies 1 - Tortora unpublished MSc thesis; 2 - Pappalardo et
1370 al. (1999); 3 - Arienzo et al. (2009), resampled 10/2008; 4 - Polacci et al. (2003).
1371 Ages are from: PP - Smith et al. (2011), NYT- De Vivo et al. (2001), CI - Deino et
1372 al. (2004) PRa, VRb and TLa - Pappalardo et al. (1999). Mineral abbreviations:
1373 san – sanidine, plg – plagioclase, cpx – clinopyroxene, bt - biotite, mag -
1374 magnetite, ap - apatite, ol - olivine.

1375

1376 Table 2: Representative EMPA analyses of volcanic glass selected on basis of
1377 CaO (20th, 40th, 60th, 80th percentile for most samples, 33th and 66th percentiles
1378 for each mode of bimodal units) and ordered by increasing CaO. Major element
1379 totals are normalised to 100 wt%, the pre-normalised total is also given. a) PP,
1380 NYT and Pre-NYT eruptions; b) CI and Pre-CI eruptions. The full dataset is given
1381 as online supplementary data.

1382

1383 Table 3: Representative LA-ICP-MS analyses of volcanic glass selected on basis
1384 of Sr (20th, 40th, 60th, 80th percentile for most samples, 33th and 66th percentiles
1385 for each mode of bimodal units): a) PP, NYT and Pre-NYT eruptions; b) CI and
1386 Pre-CI eruptions. The full dataset is given as online supplementary data.

1387

1388 Table 4: Representative major (EMPA) and trace (LA-ICP-MS) element
1389 composition of glass shards from Lago Grande di Monticchio tephra units.

1390

1391 Table 5: Key concentrations and ratios for geochemical fingerprinting. *Total
1392 Alkali (Na₂O+K₂O) versus Silica (SiO₂) (Le Bas and Streckeisen, 1991).

1393

1394 Table 6: Summary of information relevant to proximal-medial-distal correlations.
1395 Ages have been calibrated using the IntCal09 or Marine09 internationally
1396 accepted calibration curves (Reimer et al., 2009) at 2σ. Year 0 is 1950 AD.
1397 Please see references for uncalibrated radiocarbon determinations. Distal tephra
1398 occurrences are those supported by this study, in the case of the CI only studies
1399 with trace element data are listed.

1400

1401 **Figures**

1402

1403 Figure 1: a) regional map of study area, inset shows location of: b) Map of field
1404 localities modified after Orsi et al. (2003).

1405

1406 Figure 2: Total alkali-silica plot (Le Bas and Streckeisen, 1991) showing the CI-
1407 series (red/orange), NYT-series (blues) and PP (green). Also shown are distal
1408 tephra layers from the Lago Grande di Monticchio core (black). Errors are 2 s.d.
1409 calculated using replicate analyses of MPI-DING StHs6/80 glass.

1410

1411 Figure 3: Major element biplots showing normalised compositions of glasses from
1412 the CI-series (red/orange), NYT-series (blues) and PP (green). Also shown are
1413 distal tephra layers from the Lago Grande di Monticchio core (black). Errors are 2
1414 s.d. calculated using replicate analyses of MPI-DING StHs6/80 glass.

1415
1416 Figure 4: Primitive mantle normalised trace element compositions of a) NYT and
1417 PP; and b) Pre-NYT (NYT range shown for comparison); c) CI; and d) Pre-CI (CI
1418 range shown for comparison) units. Primitive mantle values are from Sun and
1419 McDonough (1989).

1420
1421 Figure 5: Trace element compositions of members of the PP (green), NYT-series
1422 (blues) and CI-series (red/orange). Also shown are distal tephra layers from the
1423 Lago Grande di Monticchio core (black). Reproducibility (2 s.d.) of StHs6/80-G
1424 (S) and ATHO-G (A) analyses are shown.

1425
1426 Figure 6: Discriminating the fall and lower/intermediate phases of the CI using Zr-
1427 Th. Line points are 35, 495 and 65, 770.

1428
1429 Figure 7: Trace element compositions of Lago Grande di Monticchio tephra
1430 normalised to the average composition (grey field) and compared to
1431 representative proximal compositions (10th, 20th, 30th, 40th, 50th, 60th, 70th, 80th,
1432 90th Sr percentile where >20 analyses): a) TM-7b and PP; b) TM-8 and NYT-UM;
1433 c) TM-8 and NYT-LM; d) TM15 and VRa; e) TM-18 base and CI fall; f) TM-18 top
1434 and CI flow – lower/intermediate flow.

1435
1436 Figure 8: Example biplots for assessing proximal distal tephra correlations: a)
1437 PP/TM-7b, MgO-SiO₂; b) NYT/TM-8 CaO-SiO₂; c) GM1/TM-9 K₂O-SiO₂; d)
1438 GM1/TM-9 MgO-SiO₂; e) VRa/TM15/Y3 Na₂O-SiO₂; f) VRa/TM15/Y3 FeO-SiO₂.
1439 Proximal samples (PP in green, NYT-series in blue) and Lago Grande di
1440 Monticchio (black) symbols are as in other plots. Distal marine locations are
1441 shown in red, lake settings in orange.

Table(s)

	Location	Age (ka)	Unit	Unit description	Sample name	Clast description
Pomici Principali	Via Pigna	11.92-12.26 cal BP	-	Sequence of seven pumice fall layers.	PP117 A, PP117 B3, PP117 D1, PP117 D3, PP117 D5	Beige to brown/grey, 5-10% phenocrysts, san, plg, cpx, bt, mag, minor ap, ol. Vesicularity 40-80%
	Ponti Rossi		UM	Sequence of ~4 2-4 m thick pyroclastic flows.	NYT PR UM 0301 - 0304	Yellow and brown, <3% phenocrysts, san, plg, cpx, bt, mag, minor ap. Vesicularity 60-80%.
Neapolitan Yellow Tuff	San Marco Evangelista	14.9± 0.4 ⁴⁰ Ar/ ³⁹ Ar	LM13	Pumice and ash fall, white to grey (Woeltz et al., 1995).	NYT 02 SME LM13	
	San Severino		LM3	Zoned pumice and ash fall, white to grey, normally graded (Woeltz et al., 1995).	NYT SS LM 3	Yellow-brown, <3% phenocrysts, san, plg, cpx, bt, mag, minor ap. Vesicularity 60-80%.
Pre-NYT (Tufo biancastri)	Trefola		LM1	Complex, dominated by laminated surges.	NYT TR LM 1	
	Ponti Rossi	16.1±0.2 ⁴⁰ Ar/ ³⁹ Ar	-	<0.4 m surges with intercalated fall (Orsi et al., 1996).	OCF 9602 A1 ²	light beige. <1% phenocrysts, plg, san, cpx, bt, mag, minor ap. 60-80% vesicularity.
	Verdolino	28 ka ⁴⁰ Ar/ ³⁹ Ar	-	6.0 m alternating fall and surge (Orsi et al., 1996).	OCF 945 (top), OCF 946 (base) ²	light beige. <1% phenocrysts, plg, san, cpx, bt, mag, minor ap. 60-80% vesicularity.
	Verdolino		-	4.5 m surges overlain by 0.23 m pumice fall (Orsi et al., 1996).	OCF 9603 A2, OCF 9603 A3 ²	light beige (base) to brown (top). <1% phenocrysts, plg, san, cpx, bt, mag, minor ap. 60-80% vesicularity.
	Trefola		-	1.4-1.7 m (remobilised) fall with basal surge (Orsi et al., 1996).	OCF 9542 (top) ² OCF 9544 (base) ²	light beige. <1% phenocrysts, plg, san, cpx, bt, mag, minor ap. 60-80% vesicularity.
	San Marco Evangelista			2 m thick (base not exposed), ungraded (Arienzo et al., 2009)	OF3B/08 ³	Brown-black, ca. 30% phenocrysts, san, plg, cpx, bt, mag, minor ap. Vesicularity >60%.
Campanian Ignimbrite	Mondragone		Intermediate flow	4 m thick, light to dark grey (1- thin laminated /massive, 2a, 2b - massive) (Civetta et al., 1997).	Mond15U3 ³	
	Acquafidia	39.28 ±0.11 ⁴⁰ Ar/ ³⁹ Ar	lower flow	3 m thick, grades from light brown, to reddish, to dark grey (2a, 2b - ignimbrite) (Civetta et al., 1997).	Mond15A2_08 ³	<3% phenocrysts, san, plg, cpx, bt, mag, minor ap.
Campanian Ignimbrite	Voscone		Fall	0.9 m inverse graded overlain by stratified pumice	OF 16A_08	Flow-white, vesicularity 60-90%
			Upper fall	0.4 m - stratified – Oscillatory, gradual decrease in clast size and increase in lithics (Rosi et al., 1999).	CIVOS 80-90 to 100-110 ⁴	Fall – light grey at base to pink at top. vesicularity 80-90%
			Lower fall	0.8 m - inverse graded (Rosi et al., 1999).	CIVOS 0-10 to 70-80 ⁴	
			Flow	4.0 m ignimbrite (Orsi et al 1996).	OCF 9550 ²	grey to dark grey, <1% phenocrysts, plg, san, cpx, bt, mag, minor ap. 60-80% vesicularity.
Pre-CI	Trefola		Fall	3.9 m layered fall (Orsi et al 1996).	OCF 9601 F3 ²	
	Trefola		Flow	2m pyroclastic flow (Orsi et al 1996).	OCF 9601 C24 ²	grey to dark grey, <1% phenocrysts, plg, san, cpx, bt, mag, minor ap. 60-90% vesicularity
	Trefola		Fall	13.3 m of <1.7m poorly sorted fall layers and subordinate surge beds (Orsi et al., 1996).	OCF 9601 C1 ²	
	Trefola	58.9± 1.8 ⁴⁰ Ar/ ³⁹ Ar	Flow	>1.1 m pyroclastic flow, with scoria (Orsi et al., 1996).	OCF 9601 A1 ²	grey to dark grey, <1% phenocrysts, plg, san, cpx, bt, mag, minor ap. 50-95% vesicularity.
		Fall	Poorly sorted fall, base not exposed	TLa_08		

Table(s)

Event Percen -tile	PP				NYT-UM				NYT-LM				Pre-NYT VRb				Pre-NYT PRa				Pre-NYT TLo							
	20	40	60	80	20	40	60	80	20	40	66	33	20	40	60	80	20	40	60	80	20	40	60	80				
sample	PP117 A-1	PP117 A-13	PP117 D3-2	PP117 D5-27	NYT PR UM 0301-3	NYT PR UM 0301-2	NYT PR UM 0302-2	NYT PR UM 0304-17	NYT TR LM1-1	NYT TR LM1-7	NYT 02 SME LM13-6	NYT 02 SME LM13-1	OCF 945-3	OCF 946-1	OCF 945-1	OCF 945-9	9603 A3-9	9603 A3-8	9603 A2-6	9603 A2-10	OCF9602 A1-19	OCF9602 A1-9	OCF9602 A1-25	OCF9602 A1-13	OCF 9544-2	OCF 9544-5	OCF 9542-5	OCF 9542-8
Total	95.03	96.63	95.05	96.51	97.00	97.00	99.54	97.64	96.91	97.77	98.24	97.98	96.29	95.55	97.17	95.90	99.16	97.58	96.13	95.60	96.63	95.48	95.63	96.02	95.79	97.27	96.38	95.48
SiO ₂	58.21	58.26	57.84	57.83	61.75	59.72	58.90	55.76	61.46	61.79	58.19	57.61	62.34	62.21	62.40	62.14	58.33	58.09	62.59	62.21	62.51	62.64	62.41	62.43	64.04	63.68	63.92	63.75
TiO ₂	0.52	0.49	0.54	0.54	0.45	0.47	0.51	0.54	0.37	0.38	0.65	0.68	0.43	0.47	0.46	0.46	0.67	0.68	0.42	0.46	0.40	0.37	0.35	0.36	0.39	0.41	0.40	0.39
Al ₂ O ₃	18.98	18.88	18.91	19.04	18.19	19.01	18.90	19.91	18.90	18.55	18.51	18.73	18.41	18.30	18.08	18.49	18.33	18.30	18.11	18.14	18.35	18.22	18.39	18.53	18.04	18.05	17.98	18.22
MnO	0.14	0.12	0.19	0.10	0.15	0.13	0.22	0.23	0.12	0.15	0.19	0.13	0.10	0.11	0.20	0.15	0.14	0.17	0.15	0.13	0.10	0.03	0.13	0.12	0.18	0.21	0.24	0.17
MgO	1.06	1.01	1.19	1.27	0.49	0.71	1.09	1.55	0.40	0.44	1.23	1.33	0.40	0.43	0.42	0.33	1.35	1.52	0.43	0.43	0.36	0.40	0.42	0.37	0.21	0.21	0.22	0.22
FeO	4.38	4.28	4.59	4.58	2.80	3.45	4.04	5.39	2.65	2.90	4.87	4.86	2.42	2.62	2.52	2.47	5.13	5.30	2.81	2.84	2.66	2.58	2.78	2.64	2.30	2.51	2.31	2.35
CaO	3.67	3.78	3.91	4.12	2.30	2.75	3.45	4.67	2.18	2.15	4.22	4.30	2.13	2.24	2.26	2.31	3.95	4.04	2.20	2.23	2.10	2.19	2.24	2.33	1.45	1.48	1.49	1.52
Na ₂ O	3.51	3.65	3.50	3.54	4.44	3.45	3.68	3.40	4.35	4.47	3.50	3.56	4.73	4.38	4.69	4.61	3.34	3.26	4.32	4.24	4.69	4.69	4.23	3.89	6.13	6.17	5.97	5.93
K ₂ O	8.96	9.02	8.82	8.48	8.95	9.93	8.88	8.13	9.06	8.62	8.25	8.42	8.59	8.83	8.51	8.58	8.37	8.24	8.45	8.83	8.37	8.37	8.64	8.90	6.64	6.62	6.83	6.83
Cl	0.58	0.51	0.51	0.51	0.50	0.38	0.33	0.37	0.52	0.55	0.39	0.38	0.46	0.40	0.45	0.46	0.40	0.39	0.52	0.50	0.45	0.51	0.41	0.43	0.64	0.66	0.63	0.63

Event Percen -tile	sample	CI upper flow				CI lower/intermediate flow				CI fall				Pre-CI TLI				Pre-CI TLc				Pre-CI TLa			
		20	40	60	80	20	40	60	80	20	40	60	80	20	40	60	80	20	40	60	80	20	40	60	80
Total		96.23	95.95	97.18	97.00	97.25	95.21	97.93	96.58	97.16	95.45	95.75	95.96	99.47	97.18	96.77	97.47	98.17	98.47	99.18	98.11	96.44	96.16	100.3	96.17
SiO ₂		62.93	62.10	61.63	61.58	61.78	61.03	61.50	61.24	60.83	61.81	60.89	61.37	59.05	59.56	59.33	59.36	58.43	58.49	58.46	58.28	59.11	58.91	58.75	59.25
TiO ₂		0.43	0.45	0.44	0.42	0.41	0.45	0.42	0.45	0.47	0.44	0.46	0.40	0.42	0.37	0.41	0.40	0.38	0.39	0.41	0.37	0.42	0.39	0.38	0.38
Al ₂ O ₃		18.29	18.78	18.65	18.35	18.71	18.93	18.95	18.74	19.35	19.04	19.50	18.69	20.00	19.73	19.85	19.84	19.64	19.91	19.81	19.88	19.70	19.71	19.64	19.58
MnO		0.17	0.21	0.08	0.09	0.24	0.15	0.17	0.23	0.19	0.20	0.24	0.25	0.21	0.23	0.24	0.24	0.27	0.23	0.25	0.29	0.25	0.29	0.28	0.30
MgO		0.38	0.36	0.76	0.77	0.32	0.28	0.35	0.32	0.32	0.33	0.34	0.33	0.35	0.39	0.39	0.37	0.31	0.30	0.29	0.31	0.32	0.31	0.31	0.35
FeO		2.95	2.74	3.31	3.48	2.92	2.72	2.96	2.93	2.93	2.90	2.95	2.90	3.26	3.27	3.28	3.30	3.58	3.57	3.42	3.59	3.44	3.43	3.54	3.47
CaO		1.39	1.55	1.77	2.09	1.60	1.66	1.70	1.72	1.71	1.75	1.78	1.83	2.01	2.08	2.10	2.13	2.01	2.04	2.06	2.11	1.88	1.94	1.98	2.04
Na ₂ O		4.51	4.43	3.39	3.16	5.89	6.54	5.75	6.36	6.18	6.12	6.11	6.13	5.96	5.72	5.88	5.81	7.11	6.72	7.16	6.93	6.89	6.77	6.92	6.63
K ₂ O		8.47	8.76	9.72	9.82	7.28	7.35	7.42	7.17	7.35	6.81	7.14	7.43	7.98	7.90	7.77	7.83	7.39	7.54	7.34	7.38	7.34	7.44	7.40	7.20
Cl		0.46	0.62	0.26	0.25	0.85	0.89	0.78	0.84	0.66	0.62	0.60	0.66	0.76	0.75	0.74	0.73	0.86	0.82	0.82	0.83	0.71	0.80	0.79	0.79

Table(s)

Event Percentile	PP								NYT-UM				NYT-LM				Pre-NYT VRb				Pre-NYT VRa				Pre-NYT PRa				Pre-NYT TLo			
	20	40	60	80	20	40	60	80	20	40	60	80	20	40	60	80	20	40	60	80	20	40	60	80	20	40	60	80	20	40	60	80
sample	PP117 D1-30	PP117 08A-20	PP117 B3-8c	PP117 08A-2	NYT PR UM 0301-13	NYT PR UM 0304-14	NYT PR UM 0302-14	NYT PR UM 0302-5	NYT TR LM1-2	NYT TR LM1-4	NYT SS LM3-8	NYT2 SME LM13-4	OCF 945-4	OCF 945-8	OCF 946-9	OCF 946-8	OCF 9603 A3-3	OCF 9603 A3-10	OCF 9603 A2-7	OCF 9603 A2-10	OCF 9602 A1-19a	OCF 9602 A1-12	OCF 9602 A1-14b	OCF 9602 A1-6a	OCF 9544-10	OCF 9542-4	OCF 9542-6	OCF 9542-10				
Ti	2451	2719	2492	2773	2618	2505	2835	2745	2603	2601	3272	3386	2632	2681	2368	2505	3413	3383	2315	2291	2489	2497	2425	2313	2361	2294	2458	2484				
V	100	110	97	110	55	86	91	93	56	58	119	135	53	49	51	56	113	113	38	37	56	54	54	49	23	24	27	24				
Rb	364	376	368	366	393	342	319	320	386	381	336	314	374	386	377	358	328	323	356	359	353	383	380	376	527	523	476	533				
Sr	819	844	858	872	244	527	901	1066	259	286	755	804	162	176	248	315	736	708	276	236	329	272	246	236	16	19	21	22				
Y	24	22	26	24	33	20	23	22	35	33	28	25	34	36	27	31	24	25	29	29	30	32	33	30	55	47	52	50				
Zr	257	232	265	239	368.4	222	226	216	396	374	299	260	367	395	299	338	262	260	325	329	332	341	351	328	840	701	766	719				
Nb	42	42	44	42	59.1	40	36	34	62	61	48	43	61	62	55	54	41	39	49	50	53	55	56	54	119	111	113	109				
Ba	1680	1780	1776	1802	87.7	923	1382	1656	93	144	1321	1454	39	43	100	160	1267	1259	108	74	222	140	103	112	4	5	5	5				
La	62	59	64	60	82.7	56	57	56	86	83	72	65	79	87	67	76	48	51	66	66	74	81	84	72	148	126	130	131				
Ce	120	113	121	117	161	106	111	108	166	159	143	128	152	168	128	145	95	101	125	126	142	149	163	142	267	240	247	239				
Pr	13	12	13	12	17	11	12	12	17	16	15	13	17	17	13	15	10	11	13	13	14	17	17	15	26	23	24	23				
Nd	46	45	48	44	61.3	40	44	43	62	59	54	51	56	61	48	55	39	41	47	49	52	58	59	54	85	77	76	79				
Sm	8.4	<LOD	8.4	9.6	9.5	<LOD	7.9	7.5	11.4	11.2	10.1	9.3	<LOD	10.8	<LOD	8.8	<LOD	8.2	9.3	7.9	9.1	10.4	11.4	9.3	13.7	12.8	12.2	11.6				
Eu	2.0	2.1	2.0	2.0	2.0	<LOD	2.2	2.2	2.1	1.9	2.2	2.1	<LOD	2.1	<LOD	2.0	<LOD	1.9	1.9	1.8	1.9	2.1	2.1	1.8	1.2	1.1	1.2	1.1				
Gd	6.2	<LOD	6.7	<LOD	7.2	6.8	5.3	5.7	7.9	<LOD	7.3	6.6	8.5	7.6	<LOD	7.6	<LOD	5.9	6.5	6.3	6.9	7.5	8.0	8.0	9.9	9.1	10.5	9.3				
Dy	4.5	4.4	4.9	4.6	6.1	3.7	4.1	4.4	6.7	6.1	5.9	5.1	6.3	6.6	<LOD	5.7	<LOD	4.7	5.2	5.2	5.7	6.4	6.6	5.3	9.0	8.2	8.5	7.9				
Er	2.2	<LOD	2.8	2.1	3.2	<LOD	2.1	2.1	3.4	3.3	2.9	2.5	3.0	3.4	<LOD	3.0	<LOD	2.5	2.8	2.9	3.0	3.3	3.4	3.2	5.4	4.8	5.2	4.6				
Yb	2.3	<LOD	2.5	<LOD	3.1	2.3	2.0	2.0	3.2	3.2	2.9	2.4	<LOD	3.3	<LOD	3.1	<LOD	2.5	2.8	2.9	3.1	3.2	3.3	2.7	6.2	5.4	5.5	5.0				
Lu	0.4	<LOD	0.4	<LOD	0.4	<LOD	0.3	0.3	0.5	0.5	0.4	0.4	<LOD	0.5	<LOD	0.4	<LOD	0.3	<LOD	0.4	0.4	0.4	0.4	0.4	0.9	0.8	0.7	0.8				
Ta	2.1	1.8	2.2	1.7	2.9	1.8	1.8	1.6	3.0	2.9	2.4	2.0	2.4	3.0	2.4	2.8	<LOD	2.0	2.2	2.5	2.6	2.6	2.9	2.6	5.1	4.7	5.3	4.4				
Th	24	20	26	22	35	20	21	20	37	35	29	25	30	36	25	32	21	22	25	27	31	32	33	31	79	68	70	63				
U	8	7	9	8	11	8	7	7	12	11	9	8	9	12	9	10	7	8	8	9	10	10	10	10	26	23	24	23				

Continues next page

Event Percentile	Cl upper flow				Cl lower/intermediate flow				Cl fall				Pre-Cl Tlf				Pre-Cl TLC				Pre-Cl Tla							
	80	60	40	20	80	60	40	20	80	60	40	20	80	60	40	20	80	60	40	20	80	60	40	20	80	60	40	20
Sample	OCF 9601 A1-20	OCF 9601 A1-19	OCF 9601 A1-10	OCF 9601 A1-6	OCF 9601 A1-17	OCF 9601 A1-10	OCF 9601 A1-7	OCF 9601 A1-6	OCF 9601 A1-10	OCF 9601 A1-10	OCF 9601 A1-7	OCF 9601 A1-6	OCF 9601 A1-6	OCF 9601 A1-10	OCF 9601 A1-7	OCF 9601 A1-6	OCF 9601 A1-6	OCF 9601 A1-6	OCF 9601 A1-6	OCF 9601 A1-10	OCF 9601 A1-7	OCF 9601 A1-6	OCF 9601 A1-6	OCF 9601 A1-10	OCF 9601 A1-7	OCF 9601 A1-6	OCF 9601 A1-6	OCF 9601 A1-6
Ti	2314	2352	2304	2361	2308	2210	2334	2275	2436	2741	2351	2253	2356	2501	2532	2380	2234	2289	2361	2164	2275	2183	2205	2231	2275	2183	2205	2231
V	64	37	28	22	14	13	14	13	14	14	16	16	21	21	21	22	14	12	13	12	13	13	12	13	13	13	12	13
Rb	324	373	437	382	436	453	447	434	420	487	473	465	447	426	418	436	476	460	453	466	494	468	460	467	494	468	460	467
Sr	378	233	71	42	44	39	28	25	65	36	33	25	41	35	32	30	15	15	14	13	16	15	14	14	16	15	14	14
Y	20	32	36	50	50	49	52	46	49	54	52	51	44	47	47	46	57	61	60	56	61	60	61	62	61	60	61	62
Zr	173	335	405	598	610	582	616	560	660	660	650	615	527	580	569	548	746	762	751	704	761	748	768	780	761	748	768	780
Nb	29	61	74	114	115	110	113	112	119	120	119	117	101	109	107	107	144	145	145	142	145	146	149	151	145	146	149	151
Ba	573	251	73	34	15	19	15	17	32	33	22	19	16	9	9	8	10	6	6	6	9	6	6	6	9	6	6	6
La	44	72	85	121	119	115	119	113	115	128	125	121	106	117	114	111	136	142	141	132	144	142	146	147	144	142	146	147
Ce	83	139	162	232	230	219	229	215	200	238	235	231	209	220	213	214	267	272	270	253	277	275	282	289	277	275	282	289
Pr	9	14	16	23	23	22	23	22	22	25	24	23	21	23	21	21	26	28	27	25	27	27	28	29	27	27	28	29
Nd	33	51	59	80	80	75	80	72	73	85	84	81	72	77	74	74	90	93	94	87	96	93	97	98	96	93	97	98
Sm	6.1	8.5	10.4	14.4	13.4	13.2	13.5	11.8	13.4	15.2	14.7	13.8	13.2	13.2	12.8	12.5	15.4	15.7	15.9	14.0	16.3	15.9	17.4	16.9	16.3	15.9	17.4	16.9
Eu	2.0	1.6	1.6	1.3	1.4	1.2	1.3	1.3	1.1	1.2	1.3	1.3	1.7	1.8	1.7	1.6	1.4	1.6	1.5	1.3	1.4	1.5	1.5	1.6	1.4	1.5	1.5	1.6
Gd	4.4	7.3	7.6	10.0	10.7	9.9	9.8	9.9	10.1	11.1	10.2	10.5	9.6	10.1	9.6	9.5	12.1	12.0	11.3	10.5	11.9	12.7	12.6	12.4	11.9	12.7	12.6	12.4
Dy	3.7	5.7	6.6	8.9	9.0	8.6	9.3	8.5	8.5	10.0	9.7	9.4	7.9	8.6	8.7	8.0	10.0	10.8	10.8	10.0	10.7	10.7	11.0	11.3	10.7	10.7	11.0	11.3
Er	1.9	3.2	3.6	5.1	5.2	5.0	5.3	4.9	4.8	5.5	5.1	5.0	4.4	4.9	4.8	4.7	6.0	6.0	5.8	5.6	6.1	6.0	6.1	6.2	6.1	6.0	6.1	6.2
Yb	1.8	3.1	3.7	5.1	5.5	4.9	5.4	4.6	4.7	5.6	5.6	5.5	4.1	4.7	4.8	4.6	5.6	6.2	6.1	5.5	5.9	6.3	6.3	6.3	5.9	6.3	6.3	6.3
Lu	0.3	0.5	0.5	0.7	0.8	0.8	0.7	0.7	0.7	0.8	0.8	0.8	0.6	0.7	0.7	0.6	0.9	0.9	0.9	0.8	0.9	0.9	0.9	1.0	0.9	0.9	0.9	1.0
Ta	1.4	3.2	3.5	5.5	5.4	5.0	5.3	4.9	5.7	5.5	5.7	5.5	4.6	5.2	5.0	5.0	6.6	7.0	6.8	6.5	6.7	6.8	7.0	7.2	6.7	6.8	7.0	7.2
Th	14	26	32	47	50	45	49	43	46	50	51	50	41	45	45	44	57	60	58	53	59	60	62	63	59	60	62	63
U	5	10	12	18	18	16	18	16	15	17	19	19	15	16	16	16	22	22	21	21	22	23	23	23	22	23	23	23

Sample Shard	TM-7b (PP)				TM-8 (NYT)				TM-9 (Pre-NYT)				TM-15 (Pre-NYT)							
	7b-4	7b-5	7b-4	7b-8	7b-15	8-5	8-7	8-12	8-9	8-10	9-1	9-34	9-4	9-6	9-7	15-1	15-2	15-3	15-4	15-5
EMPA (wt. % oxide)																				
Total	96.23	95.23	96.23	97.66	98.07	97.09	97.23	96.04	96.71	95.82	95.31	99.11	97.49	98.33	98.53	96.38	97.70	95.68	96.50	96.27
SiO ₂	57.51	58.15	57.51	57.35	57.71	61.81	56.20	56.90	56.39	61.63	62.99	62.58	62.71	62.85	62.74	62.88	62.54	62.26	62.14	62.19
TiO ₂	0.52	0.49	0.52	0.55	0.51	0.41	0.59	0.58	0.64	0.45	0.43	0.48	0.44	0.44	0.45	0.36	0.34	0.37	0.37	0.37
Al ₂ O ₃	19.06	18.92	19.06	19.08	19.07	19.13	18.50	18.52	18.49	18.46	18.00	18.06	18.13	18.22	18.24	17.85	17.83	17.84	18.16	17.84
MnO	0.13	0.19	0.13	0.12	0.11	0.13	0.11	0.08	0.19	0.11	0.19	0.16	0.18	0.15	0.15	0.12	0.10	0.14	0.14	0.12
MgO	1.20	1.13	1.20	1.31	1.13	0.29	2.08	1.57	1.91	0.43	0.30	0.27	0.30	0.27	0.24	0.45	0.47	0.56	0.60	0.61
FeO	4.50	4.41	4.50	4.81	4.48	2.35	5.87	5.44	5.79	2.80	2.40	2.55	2.49	2.48	2.52	3.01	2.95	3.04	3.25	3.06
CaO	3.92	3.83	3.92	4.07	3.88	2.37	5.50	4.89	5.20	2.22	1.93	1.83	1.98	1.88	1.88	2.15	2.21	2.25	2.48	2.41
Na ₂ O	3.63	3.40	3.63	4.04	3.75	4.06	3.19	3.15	3.05	4.56	5.46	5.33	5.24	5.18	5.22	4.13	4.29	3.77	3.62	3.62
K ₂ O	8.88	8.82	8.88	7.97	8.70	9.03	7.62	8.47	7.92	8.77	7.60	7.98	7.80	7.82	7.83	8.37	8.66	9.22	8.69	9.20
Cl	0.64	0.65	0.64	0.69	0.65	0.42	0.35	0.39	0.43	0.56	0.71	0.76	0.73	0.71	0.73	0.67	0.62	0.55	0.55	0.56
LA-ICP-MS (ppm)																				
Ti	2447	2290	2447	3510	3691	2204	3718	3483	3828	2328	1870	2557	2239	2358	2443	2190	2280	2188	2173	2077
V	97	91	97	125	143	51	152	145	173	54	31	37	34	35	35	37	38	44	44	43
Rb	349	327	349	268	420	370	274	303	295	402	315	404	383	390	400	335	331	307	324	260
Sr	736	680	736	722	1104	282	919	1031	1066	195	44	55	45	52	47	242	257	409	302	468
Y	23	21	23	20	30	30	24	23	26	30	34	40	35	37	36	29	28	23	24	21
Zr	230	210	230	218	323	353	209	231	229	369	377	478	425	431	425	339	328	243	273	232
Nb	39	38	39	39	56	58	33	37	37	61	66	78	74	73	73	51	49	37	47	32
Ba	1530	1399	1530	1774	2195	82	1599	2194	2060	72	7	12	6	9	6	256	169	306	402	488
La	54	50	54	53	78	79	50	58	61	81	78	98	87	88	87	66	64	53	56	48
Ce	115	101	115	104	158	150	98	114	122	155	152	192	177	180	174	125	123	100	107	91
Pr	12	11	12	11	16	16	11	12	13	16	16	18	17	17	18	13	13	10	11	9
Nd	44	38	44	42	59	57	40	46	50	57	55	68	64	65	61	49	48	43	42	35
Sm	7.9	6.9	7.9	7.6	10.4	9.2	8.4	8.3	9.6	9.5	8.5	10.7	10.7	10.6	10.5	8.5	9.5	7.2	8.9	5.3
Eu	1.8	1.5	1.8	1.8	2.6	2.1	2.0	2.2	2.3	2.1	1.4	1.9	1.5	1.7	1.5	1.8	1.8	1.7	1.5	1.7
Gd	5.8	5.4	5.8	5.3	8.1	7.6	5.5	6.3	8.1	7.3	6.9	8.6	7.9	7.5	7.0	6.2	6.2	5.5	6.7	4.7
Dy	4.1	3.4	4.1	4.1	5.7	5.5	4.6	4.6	5.2	5.6	5.8	6.9	6.1	6.7	6.5	5.3	5.2	4.3	4.6	3.9
Er	2.1	1.8	2.1	2.1	3.0	3.0	2.4	2.3	2.5	3.1	2.9	4.1	3.2	3.8	3.3	2.9	2.9	2.4	2.2	1.9
Yb	2.1	1.8	2.1	2.2	2.7	3.1	<LOD	2.1	2.2	3.0	2.6	4.2	3.7	3.4	3.5	2.9	2.8	2.1	2.4	2.3
Lu	<LOD	<LOD	<LOD	0.3	<LOD	0.5	0.4	0.3	0.4	0.4	0.5	0.5	0.6	0.5	0.5	0.4	0.4	0.3	<LOD	0.3
Ta	2.7	1.9	2.7	1.8	2.5	3.1	1.7	1.7	1.8	2.8	3.2	3.7	3.9	3.9	3.6	2.6	2.6	1.8	2.3	1.6
Th	22	19	22	21	29	35	17	21	22	34	37	44	40	41	40	30	28	20	22	18
U	8	8	8	7	11	11	5	7	7	12	11	14	13	13	13	10	9	7	8	6

Continues next page

Sample shard	TM-18 top (Cl co-ignimbrite)				TM-18 base (Cl fall)					
	18t-2	18t-3	18t-6	18t-8	18b-4	18b-9	18b-10	18b-14	18b-19	
EMPA (Wt. % oxide)										
Total	97.64	97.17	99.00	100.55	97.66	97.95	98.05	97.92	95.78	98.05
SiO ₂	61.52	61.14	61.54	61.49	61.73	61.15	61.67	61.29	61.55	61.67
TiO ₂	0.37	0.37	0.44	0.42	0.40	0.44	0.45	0.45	0.44	0.45
Al ₂ O ₃	18.58	18.18	18.66	18.32	18.21	18.53	18.41	18.20	18.30	18.41
MnO	0.22	0.13	0.28	0.20	0.30	0.24	0.19	0.20	0.28	0.19
MgO	0.30	0.81	0.33	0.28	0.32	0.29	0.31	0.33	0.35	0.31
FeO	3.06	3.39	2.90	2.98	2.84	2.96	2.85	2.86	2.90	2.85
CaO	1.65	2.75	1.63	1.66	1.68	1.75	1.63	1.75	1.72	1.63
Na ₂ O	6.28	3.41	6.62	6.38	5.79	6.66	6.42	6.85	6.41	6.42
K ₂ O	7.12	9.48	6.76	7.34	7.85	7.19	7.15	7.18	7.19	7.15
Cl	0.90	0.35	0.83	0.94	0.87	0.79	0.91	0.88	0.86	0.91
LA-ICP-MS (ppm)										
Ti	2667	2244	2590	2648	2249	2495	2518	2478	2154	2518
V	18	62	15	18	14	14	13	19	13	13
Rb	452	289	459	448	437	439	430	493	419	430
Sr	29	585	22	43	20	22	18	40	22	18
Y	54	21	56	55	47	54	50	47	45	50
Zr	639	185	667	643	569	628	626	584	549	626
Nb	118	31	120	119	103	114	113	118	99	113
Ba	50	798	17	50	24	35	14	102	48	14
La	124	45	127	125	110	123	119	115	108	119
Ce	241	88	246	243	213	234	230	224	212	230
Pr	23	10	25	24	21	24	23	24	21	23
Nd	81	36	87	83	77	81	80	73	76	80
Sm	15.0	6.5	15.1	14.1	12.7	14.1	13.1	14.7	12.1	13.1
Eu	1.4	1.8	1.4	1.5	1.3	1.4	1.2	<LOD	1.2	1.2
Gd	10.8	5.2	10.8	10.6	10.2	9.5	10.2	10.5	8.3	10.2
Dy	9.1	3.8	9.3	9.3	7.7	9.5	8.8	8.9	8.1	8.8
Er	5.0	1.8	5.7	5.0	4.4	5.1	5.0	4.9	4.2	5.0
Yb	5.2	1.7	5.5	5.2	4.5	5.7	5.3	5.2	4.2	5.3
Lu	0.8	0.3	0.8	0.8	0.7	0.8	0.8	0.6	0.6	0.8
Ta	5.9	1.5	5.9	5.5	5.0	5.2	5.3	5.3	4.3	5.3
Th	50	15	53	51	43	50	48	45	41	48
U	17	5	19	18	15	18	17	18	15	17

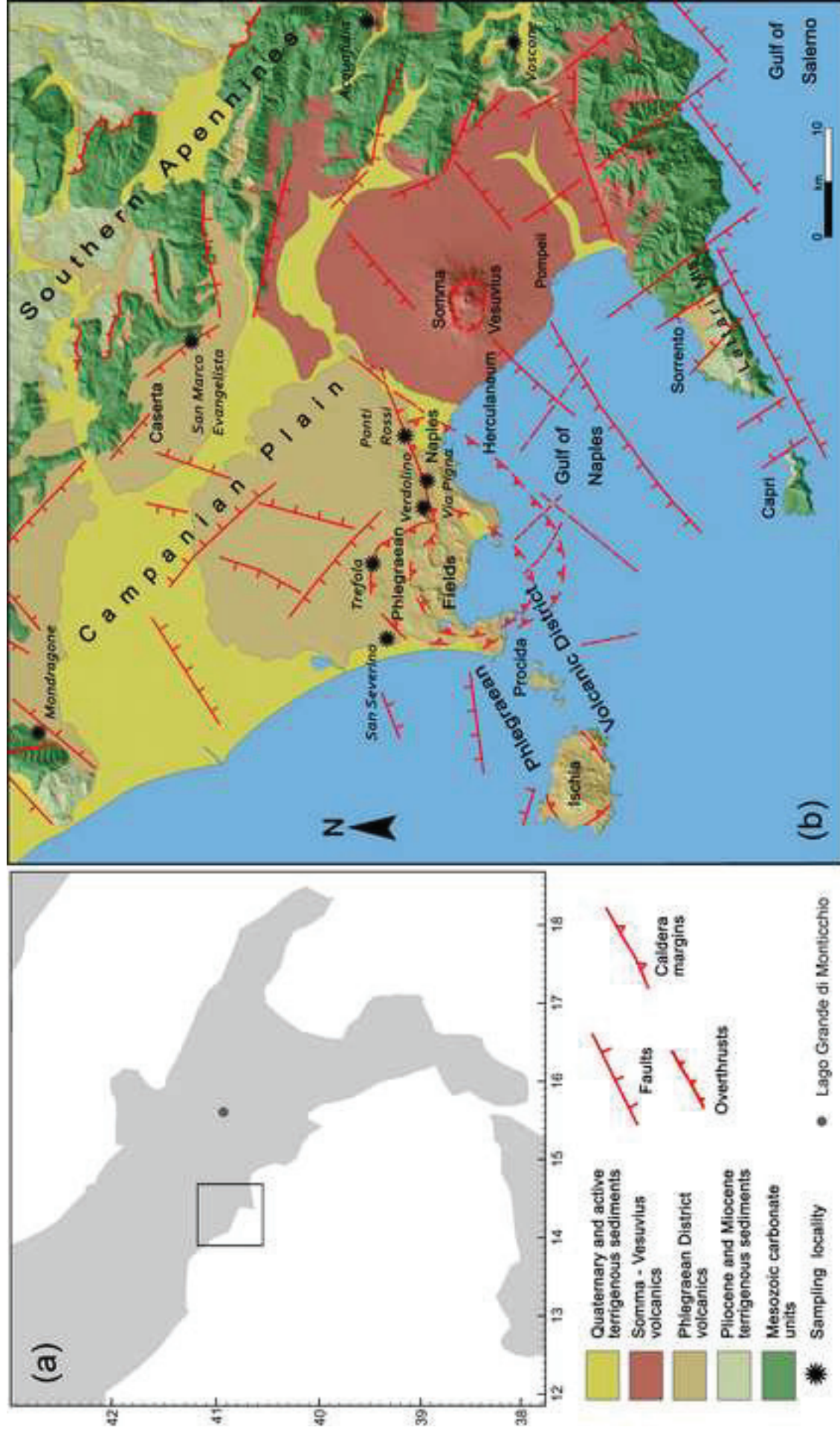
Table(s)

Sample	PP	NYT-UM		NYT-LM		Pre-NYT VRb		Pre-NYT VRa		Pre-NYT PRA		Pre-NYT TLo		CI upper flow		CI lower/intermediate flow		CI fall		Pre-CI Tlf		Pre-CI TLc		Pre-CI Tla			
		variable	variable	all	LM3, LM13	bimodal	LM1	narrow range	bimodal	A3	A2	narrow range	narrow range	narrow range	highly variable	variable	variable	variable	narrow range	narrow range	narrow range	narrow range	narrow range	narrow range	narrow range	narrow range	
Range of compositions	variable																										
Units	all	all																									
TAS* classification	phonolite	phonolite-trachyte	phonolite-trachyte	phonolite-trachyte	trachyte	trachyte	trachyte	phonolite-trachyte	trachyte	trachyte	trachyte	trachyte	trachyte	trachyte	trachyte	trachyte-phonolite	trachyte-phonolite	trachyte-phonolite	trachyte-phonolite	trachyte-phonolite	phonolite	phonolite	phonolite	phonolite	phonolite	phonolite	
Diagnostic fingerprints for PP/NYT-series and CI-series																											
FeO/CaO	1.2±0.1	1.2±0.2	1.2±0.2	1.2±0.2	1.2±0.1	1.2±0.1	1.3±0.2	1.3±0.1	1.3±0.2	1.6±0.2	1.6±0.2	1.6±0.2	1.6±0.2	1.8±0.1	1.8±0.2	1.6±0.2	1.6±0.1	1.6±0.2	1.6±0.2	1.6±0.1	1.7±0.1	1.7±0.1	1.7±0.1	1.8±0.3	1.8±0.3	1.8±0.3	1.8±0.3
Nb/Th	1.7±0.1	1.7±0.2	1.7±0.2	1.7±0.2	1.9±0.3	1.9±0.3	1.8±0.1	1.9±0.1	1.8±0.1	1.6±0.1	1.6±0.1	1.6±0.1	1.6±0.1	2.1-2.5	2.4±0.2	2.4±0.2	2.4±0.2	2.4±0.2	2.4±0.2	2.5±0.2	2.5±0.1	2.5±0.1	2.5±0.1	2.4±0.1	2.4±0.1	2.4±0.1	2.4±0.1
Zr/Th	10.5±0.5	10.6±0.7	10.8±1.0	10.8±1.0	11.2±1.1	11.2±1.1	10.7±0.4	12.1±0.7	10.7±0.4	10.5±0.6	11.8-13.4	11.8-13.4	11.8-13.4	11.8-13.4	12.7±0.6	13.2±1.1	12.8±0.5	12.8±0.5	12.8±0.5	12.8±0.5	12.9±0.6	12.9±0.6	12.9±0.6	12.5±0.4	12.5±0.4	12.5±0.4	12.5±0.4
Y/Th	1.00±0.08	1.02±0.19	1.04±0.14	1.04±0.14	1.01±0.13	1.01±0.13	0.97±0.04	1.11±0.11	0.97±0.04	0.70±0.06	1.0-1.5	1.0-1.5	1.0-1.5	1.0-1.5	1.06±0.06	1.06±0.09	1.06±0.05	1.06±0.05	1.06±0.05	1.06±0.05	1.01±0.05	1.01±0.05	1.01±0.05	0.99±0.05	0.99±0.05	0.99±0.05	0.99±0.05
Ta/Th	0.08±0.01	0.08±0.01	0.08±0.01	0.08±0.01	0.09±0.01	0.09±0.01	0.09±0.01	0.09±0.01	0.09±0.01	0.07±0.01	0.10-0.13	0.10-0.13	0.10-0.13	0.10-0.13	0.11±0.01	0.11±0.01	0.11±0.01	0.11±0.01	0.11±0.01	0.11±0.01	0.11±0.01	0.11±0.01	0.11±0.01	0.11±0.01	0.11±0.01	0.11±0.01	0.11±0.01
Cl	2.3±0.4	0.42±0.13	0.39±0.03	0.56±0.06	0.45±0.06	0.45±0.06	0.47±0.07	0.49±0.11	0.47±0.07	0.62±0.06	0.24-0.62	0.24-0.62	0.24-0.62	0.24-0.62	0.85±0.07	0.63±0.06	0.75±0.05	0.75±0.05	0.75±0.05	0.83±0.06	0.83±0.06	0.83±0.06	0.83±0.06	0.81±0.08	0.81±0.08	0.81±0.08	0.81±0.08
V	107±14	91±84	126±18	57±4	51±8	51±8	53±5	38±5	53±5	23±4	15-64	15-64	15-64	14±2	16±4	16±4	21±3	21±3	16±4	21±3	12±1	12±1	12±1	13±1	13±1	13±1	13±1
Ratios for distinguishing between series members (PP/NYT and CI)																											
Nb/Ti	0.016 ±0.003	0.017 ±0.01	0.013 ±0.002	0.023 ±0.000	0.023 ±0.002	0.023 ±0.002	0.023 ±0.002	0.012 ±0.001	0.022 ±0.004	0.048 ±0.006	0.01-0.05	0.01-0.05	0.01-0.05	0.048 ±0.004	0.047 ±0.005	0.044 ±0.003	0.044 ±0.003	0.047 ±0.005	0.044 ±0.003	0.063 ±0.003	0.063 ±0.003	0.063 ±0.003	0.066 ±0.004	0.066 ±0.004	0.066 ±0.004	0.066 ±0.004	0.066 ±0.004
Y/Ti	0.009 ±0.002	0.010 ±0.01	0.008 ±0.001	0.013 ±0.001	0.013 ±0.002	0.013 ±0.002	0.013 ±0.001	0.007 ±0.000	0.013 ±0.002	0.021 ±0.002	0.008-0.021	0.008-0.021	0.008-0.021	0.021 ±0.002	0.021 ±0.002	0.019 ±0.001	0.019 ±0.001	0.021 ±0.002	0.019 ±0.001	0.025 ±0.001	0.025 ±0.001	0.025 ±0.001	0.027 ±0.001	0.027 ±0.001	0.027 ±0.001	0.027 ±0.001	0.027 ±0.001
V/Th	4.3±0.8	3.6±4.3	4.9±1.5	1.7±0.4	1.7±0.6	1.7±0.6	1.7±0.3	5.7±1.0	1.4±0.3	0.3±0.1	0.3-4.7	0.3-4.7	0.3-4.7	0.32±0.08	0.32±0.11	0.49±0.07	0.49±0.07	0.32±0.11	0.49±0.07	0.21±0.02	0.21±0.02	0.21±0.02	0.21±0.03	0.21±0.03	0.21±0.03	0.21±0.03	0.21±0.03
Ba/Sr	1.93-2.17	0.3-2.2	1.69-1.81	0.33-0.68	0.22-0.61	0.22-0.61	0.40-0.68	1.65-1.78	0.18-0.48	0.17-0.35	0.4-1.5	0.4-1.5	0.4-1.5	0.23-1.07	0.18-1.15	0.20-0.53	0.20-0.53	0.18-1.15	0.20-0.53	0.40-0.75	0.40-0.75	0.40-0.75	0.36-0.74	0.36-0.74	0.36-0.74	0.36-0.74	0.36-0.74
Eu/Eu _N *	0.65-0.94	0.43-1.01	0.73-0.84	0.63-0.64	0.57-0.75	0.57-0.75	0.62-0.73	0.76-0.82	0.58-0.79	0.29-0.35	0.3-1.1	0.3-1.1	0.3-1.1	0.27-0.36	0.24-0.34	0.38-0.52	0.38-0.52	0.24-0.34	0.38-0.52	0.29-0.35	0.29-0.35	0.29-0.35	0.29-0.42	0.29-0.42	0.29-0.42	0.29-0.42	0.29-0.42
Zr/Sr	0.27-0.36	0.2-7.3	0.29-0.40	1.15-1.75	0.92-2.42	0.92-2.42	0.98-1.54	0.34-0.37	0.94-2.58	30-59	0-39	0-39	0-39	8-28	5-31	9-22	9-22	5-31	9-22	41-58	41-58	41-58	17-56	17-56	17-56	17-56	17-56

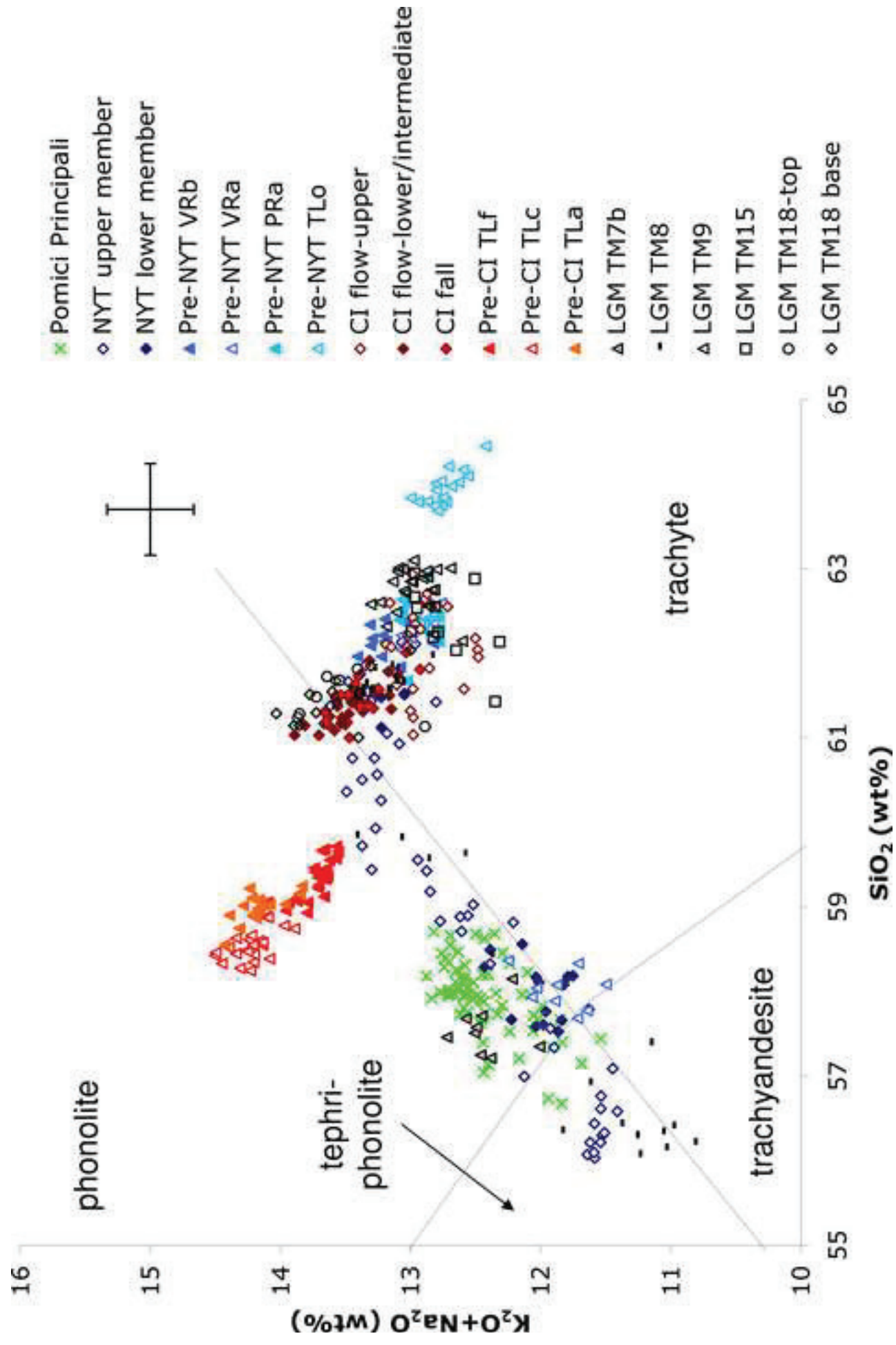
Table(s)

Event	proximal age (cal ka BP)	volume (km ³) and dispersal	distal tephra core	location	direction	Distance (km)	thickness	age (cal ka BP)	reference
PP	11.915-12.158 (¹⁴ C)	Smith et al., 2011	0.644 DRE	E	Di Rienzo et al., 2011	120	47 mm	11.571-12.789 (varve)	Wulf et al., 2004, 2008; Narcisi et al., 1996
	11.978-12.390 (Ar/Ar)	Di Vito et al., 1999	0.14 DRE	E	Lirer, 2001	310	visible		Paterne 1988
			1.78 bulk	ENE	Sulpizio, 2005	330	visible	12.003-12.579 (¹⁴ C)	Siani et al., 2004
NYT	14.500-15.300 (Ar/Ar)	Deino et al., 2004	>40 DRE	NE	Orsi, 1992	120	22 mm	13.414-14.826 (varve)	Wulf et al., 2004, 2008; Narcisi et al., 1996
NYT-LM			>10 DRE	E	Woheltz et al., 1995	310	visible		Paterne 1988
			>30 DRE	NE	Woheltz et al., 1995	200, 135	visible		Paterne 1988
NYT-UM				NE	Bourne et al., 2010	240	crypto		Bourne et al., 2010
				NE	Calanchi et al., 1998	200-240	crypto		Calanchi et al., 1998
CI	39.170-39.390 (Ar/Ar)	Di Vivo et al., 2001	105-210 DRE	NE	Pyle et al., 2006	120	257 mm fall	(170 34.934-38.611 (varve)	Wulf et al., 2004, 2008; Narcisi et al., 1996
			200 DRE	ENE to S	Rolandi et al., 2003	340	visible		Sulpizio et al., 2010; Caron et al., 2010; Wagner et al., 2008; Vogel et al., 2010
CI fall			150 DRE		Civetta et al., 1997	660	visible		Margari et al., 2007
			180-280 DRE	NE	Costa et al., 2012	1390	visible		Pyle et al., 2006
CI flow			80 bulk	E	Rosi et al., 1999	935, 970	visible		Hardiman 1999; Pyle et al., 2006
			180 bulk	ENE to S	Rolandi et al., 2003; Pyle et al., 2006	135	visible		Paterne 1988; Ton-That et al., 2001

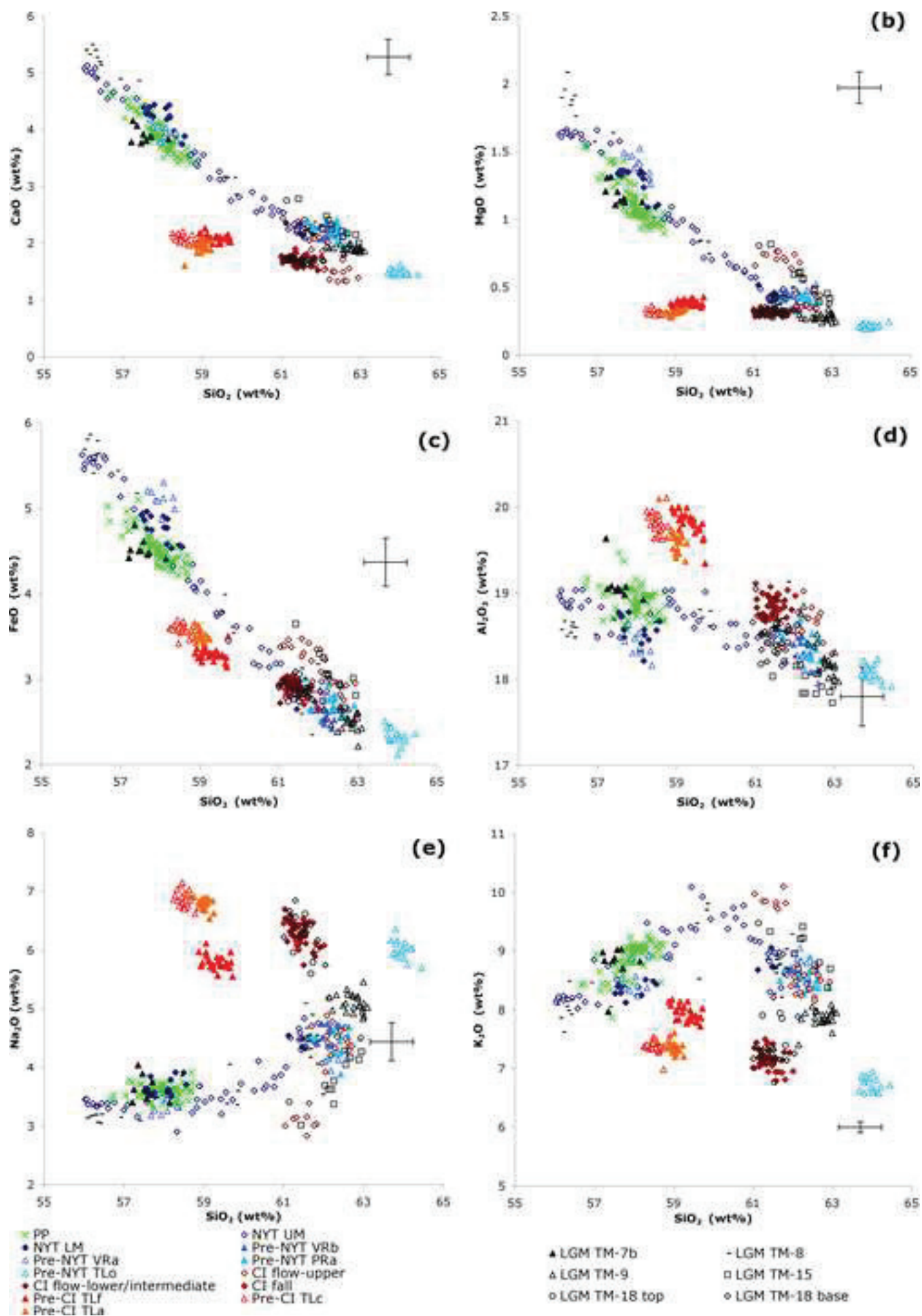
Figure(s)
[Click here to download high resolution image](#)



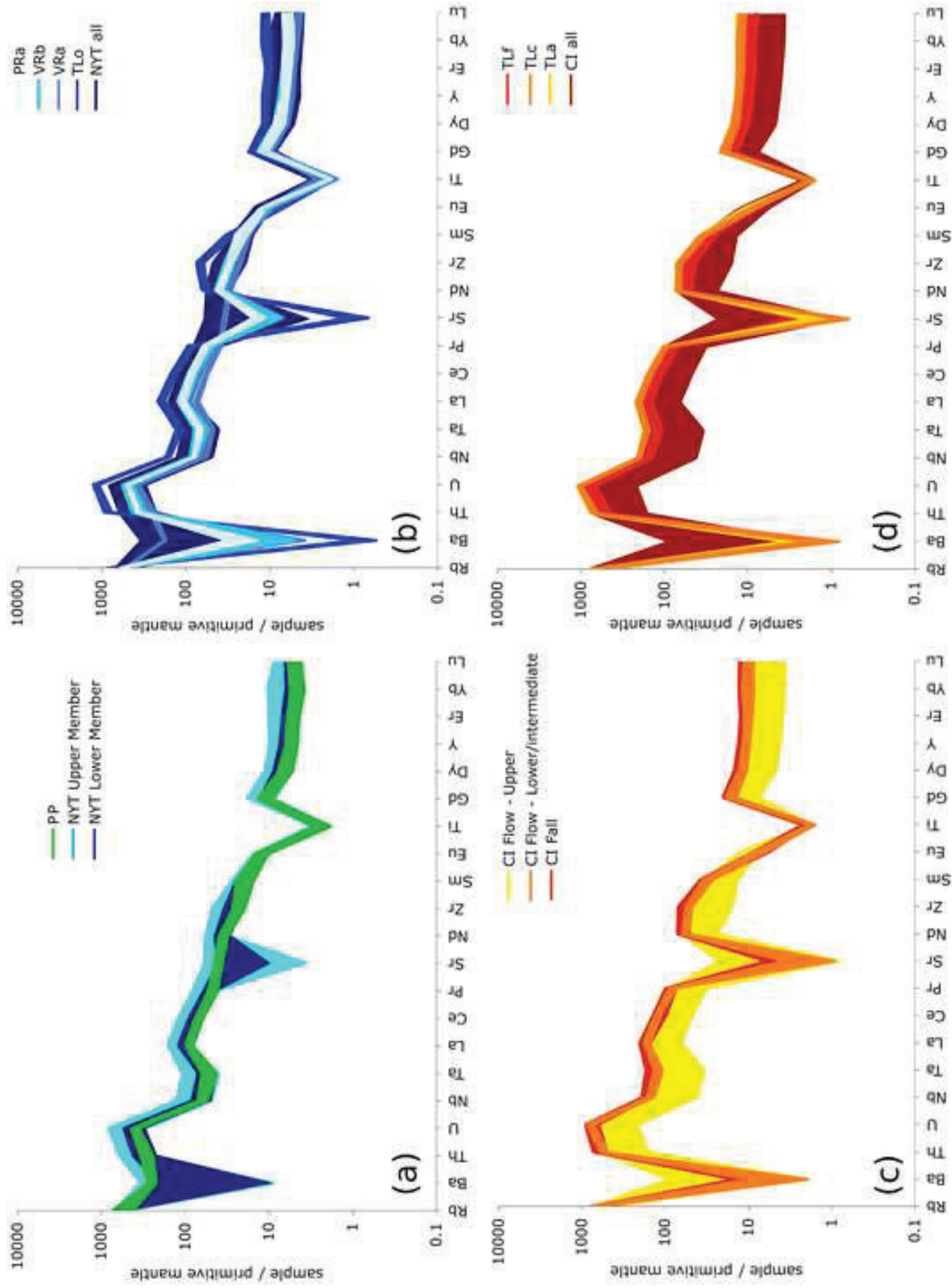
Figure(s)
[Click here to download high resolution image](#)



Figure(s)
[Click here to download high resolution image](#)

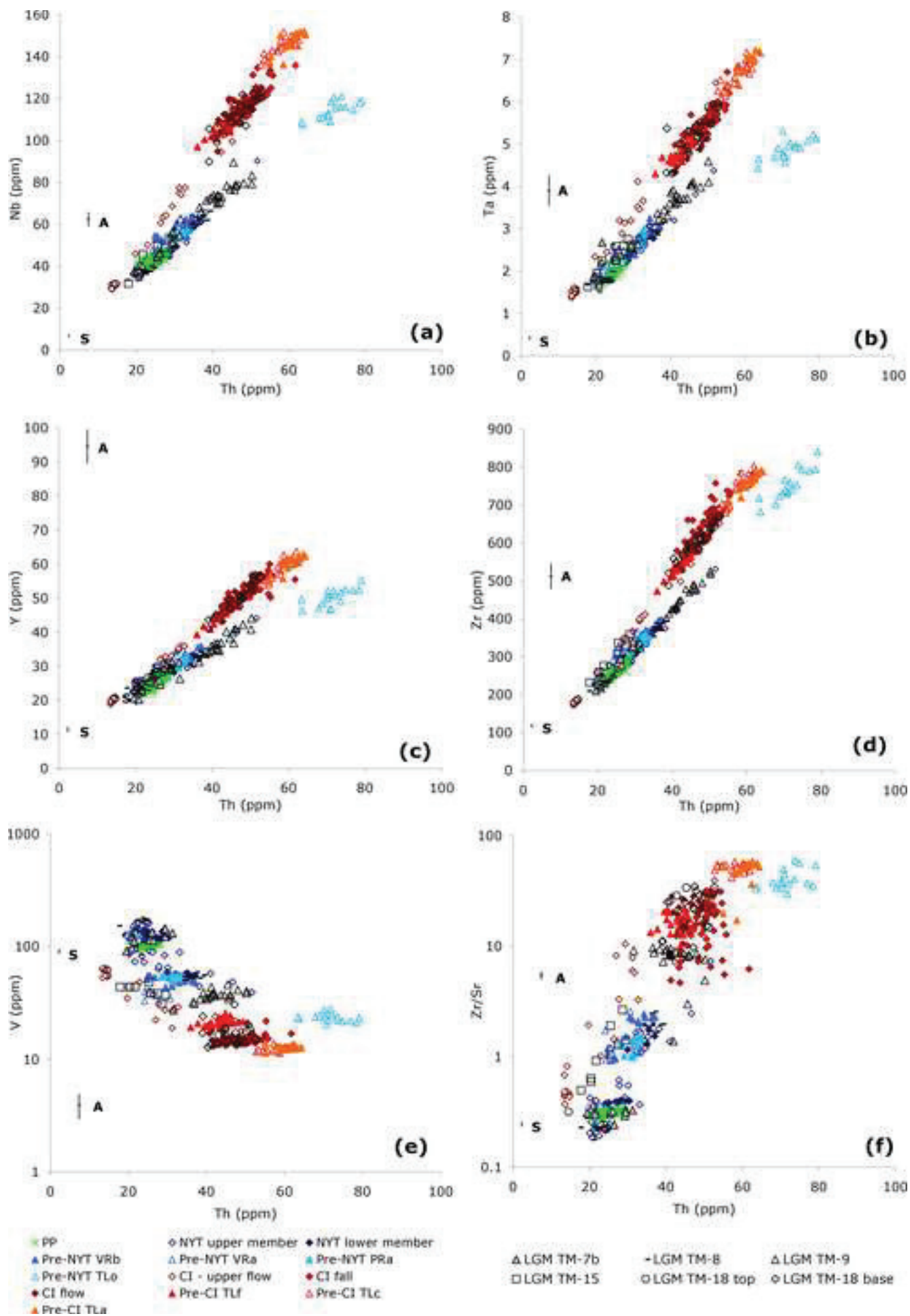


Figure(s)
[Click here to download high resolution image](#)



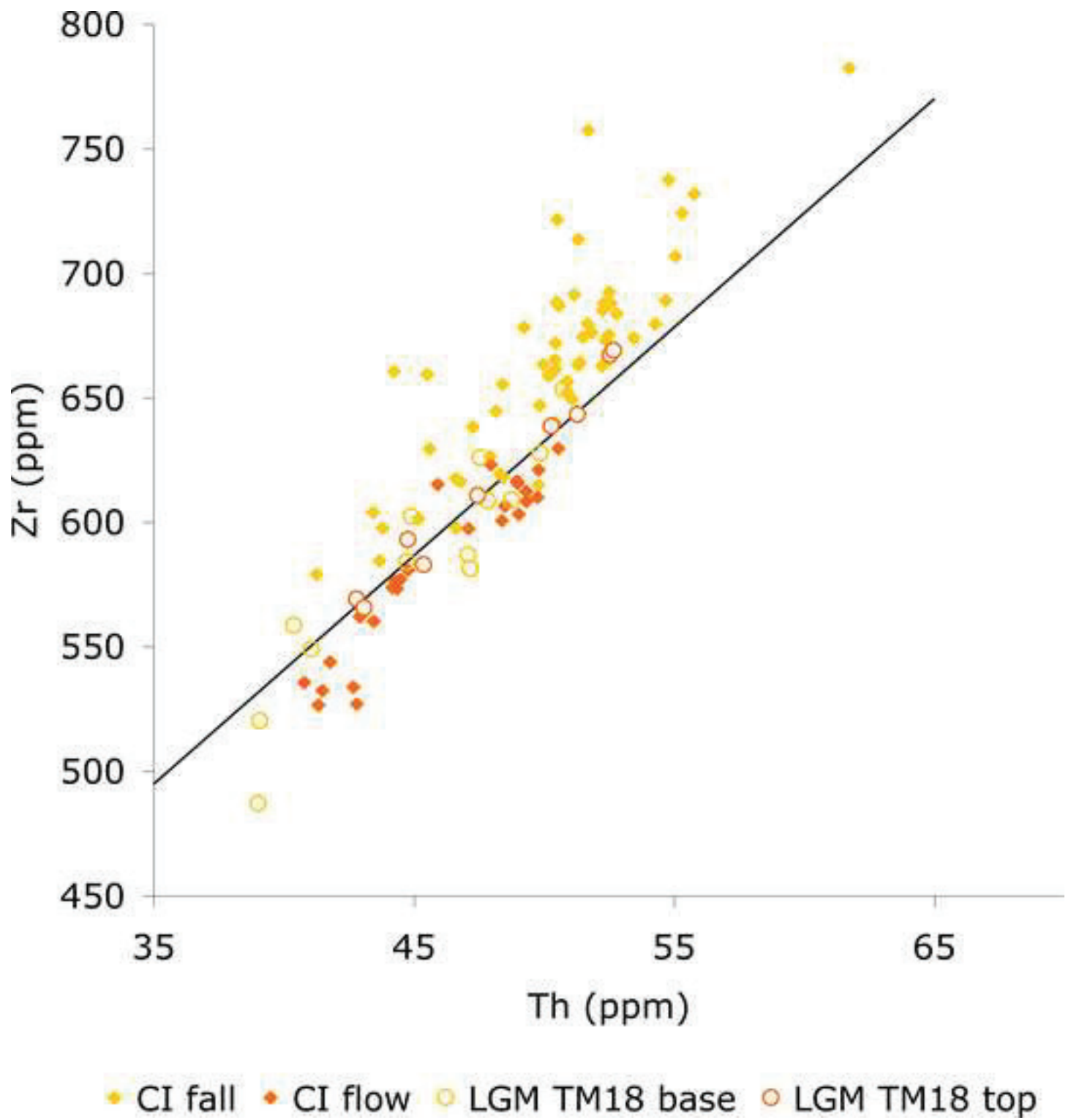
Figure(s)

[Click here to download high resolution image](#)

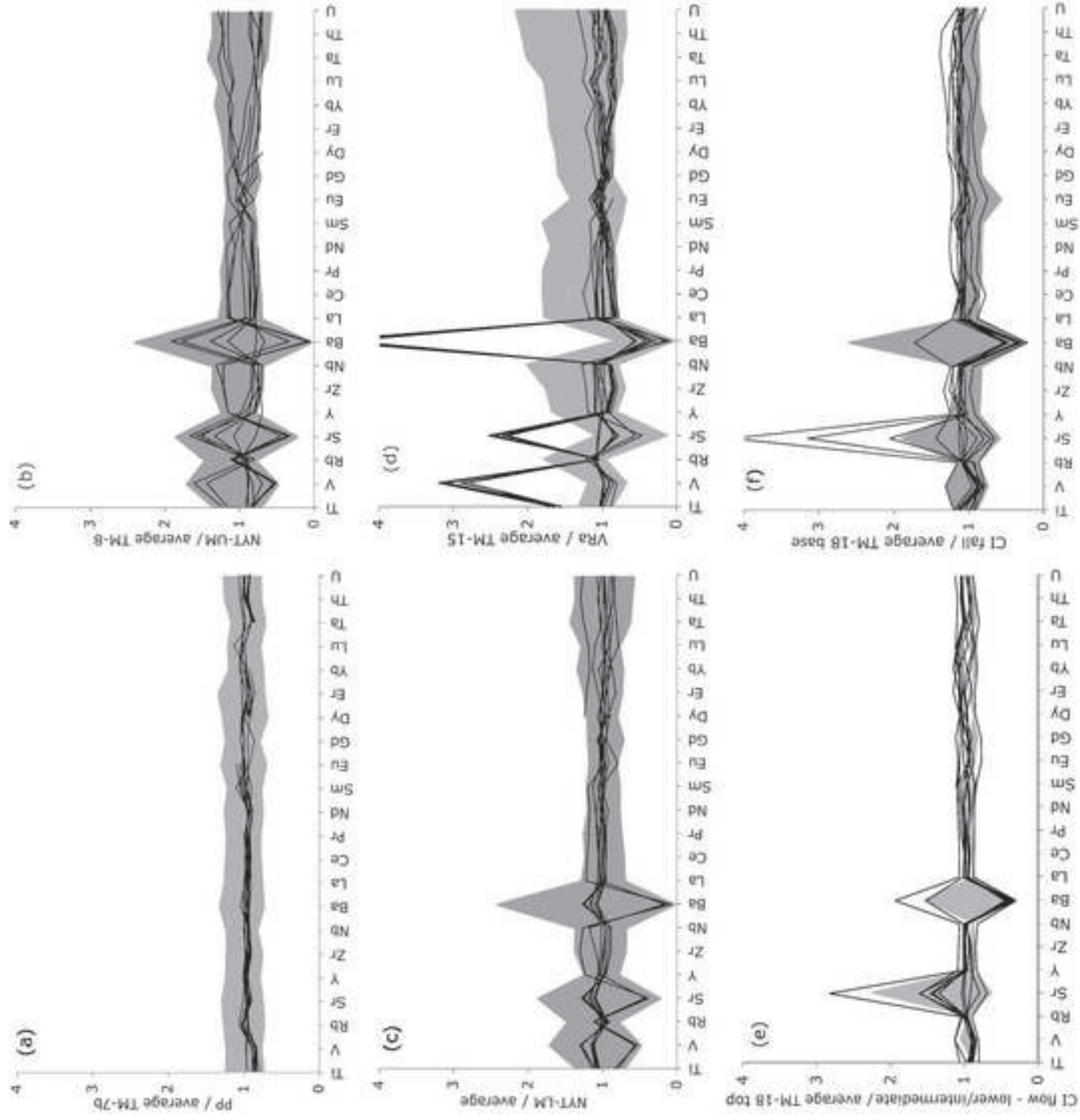


Figure(s)

[Click here to download high resolution image](#)

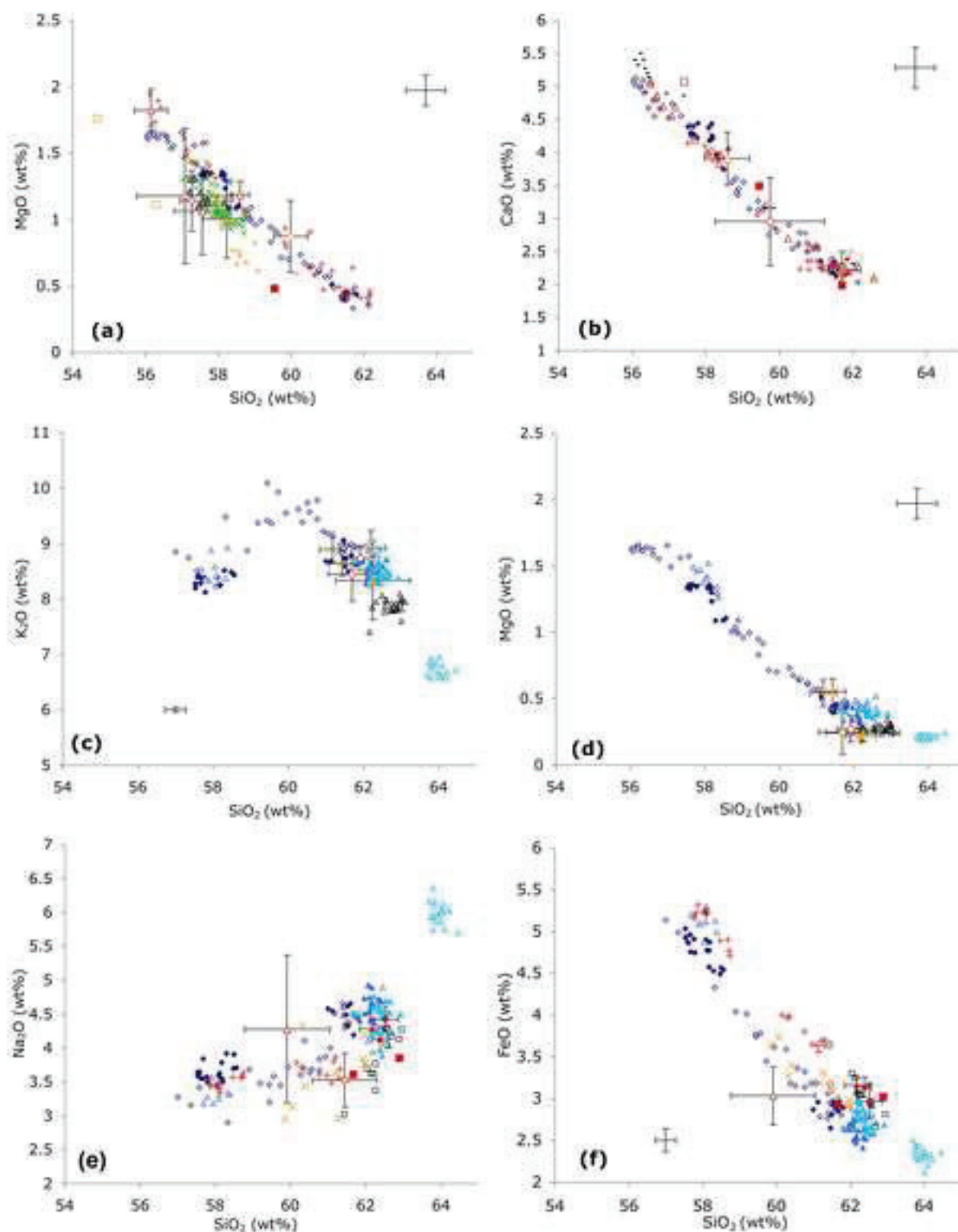


Figure(s)
[Click here to download high resolution image](#)



Figure(s)

[Click here to download high resolution image](#)



- | | | | |
|---------------------|------------|---|--|
| • Pomici Principali | ▲ LGM TM7b | ▲ GM1, Somma Vesuvius (Siani et al., 2004; Andronico et al., 1996) | ▲ Adriatic (Calanchi et al., 1998, 2008) |
| • NYT upper member | • LGM TM8 | ▲ Lake Ohrid and Prespa, Macedonia (Sulpizio et al., 2010; Caron et al., 2010; Wagner et al., 2008; Vogel et al., 2002) | □ Adriatic (Paterne 1988) |
| • NYT lower member | ▲ LGM TM9 | ▲ Langsee, Austria (Schmidt et al., 2002) | ◆ Adriatic (Siani et al., 2004) |
| ▲ Pre-NYT VRb | □ LGM TM15 | ▲ Lake Accesa, Italy (Mangy et al., 2006) | • Adriatic (Bourne et al., 2010) |
| • Pre-NYT VRa | | ▲ Lake Bled, Slovenia (Lane et al., 2011) | • Tyrrhenian (Munno and Petrosino, 2004) |
| • Pre-NYT PRa | | ▲ Lake Shkodra, Albania and Montenegro (Sulpizio et al., 2010) | • Ionian (Keller 1978) |
| • Pre-NYT TLo | | | ■ Tyrrhenian (Paterne 1988) |

Electronic Annex

[Click here to download Electronic Annex: Tomlinson_S1 \(version 2\).xls](#)